Naval Surface Warfare Center Indian Head EOD Technology Division
Indian Head, MD 20640-5035

IHTR 3827
[08Aug2019]

Soldier-Wearable, Long-Life, Low-Power Blast Sensing System Development FY15-FY19: Final Report

08 Aug 2019

Dan Jean, Ph.D (PI)
Mike Deeds, Ph.D (Branch Manager)
Scott Rauscher, Ph.D
Trong Luong
Muhammad Khan
Ralph Bridge
Matthew Winnick
Andrew Jen
Hardik Patel
Dai Dinh
and Oliver Barham, Ph.D (Author)

Members of IHEODTD E33 Branch Micro Electromechanical Systems Integrated Product Team

Sponsor: Timothy Bentley, PhD, ONR Code 34
Contract: N0001416WX00514

This page intentionally left blank

REPORT DOCUMENTATION PAGE

Form Approved
OMB No. 0704-0188

1. REPORT DATE *(DD-MM-YYYY)*	2. REPORT TYPE	3. DATES COVERED *(From - To)*
08-08-2019	Technical Report / Project Summary	FY2015 – FY2019

4. TITLE AND SUBTITLE

Soldier-Wearable, Long-Life, Low-Power
Blast Sensing System Development FY15-FY19: Final Report

5a. CONTRACT NUMBER
N0001416WX00514

5b. GRANT NUMBER

5c. PROGRAM ELEMENT NUMBER

6. AUTHOR(S)

Dan Jean, Principal Investigator, et al.

5d. PROJECT NUMBER

5e. TASK NUMBER

5f. WORK UNIT NUMBER

7. PERFORMING ORGANIZATION NAME(S) AND ADDRESS(ES)

IHEODTD
4005 Indian Head Hwy, Indian Head, MD 20640

8. PERFORMING ORGANIZATION REPORT NUMBER

3827

9. SPONSORING/MONITORING AGENCY NAME(S) AND ADDRESS(ES)

Timothy Bentley, PhD, ONR Code 34

10. SPONSOR/MONITOR'S ACRONYM(S)

ONR Code 34

11. SPONSOR/MONITOR'S REPORT NUMBER(S)

12. DISTRIBUTION/AVAILABILITY STATEMENT

Distribution A: Approved for Public Release; Distribution Unlimited.

13. SUPPLEMENTARY NOTES

14. ABSTRACT

This report summarizes work done by IHEODTD from FY15-FY19 to develop a low-power, long-life blast sensor for recording blast events potentially linked to mild traumatic brain injuries.

15. SUBJECT TERMS

16. SECURITY CLASSIFICATION OF:			17. LIMITATION OF ABSTRACT	18. NUMBER OF PAGES	19a. NAME OF RESPONSIBLE PERSON
a. REPORT	b. ABSTRACT	c. THIS PAGE			19b. TELEPHONE NUMBER *(Include area code)*

This page intentionally left blank.

FOREWORD

This work summarizes efforts by the E33 Branch Micro Electro Mechanical Systems (MEMS) Integrated Product Team of the U.S. Naval Surface Warfare Center (NSWC) Indian Head Explosive Ordnance Technology Division (IHEODTD) in developing a low-power, long life sensor suite for blast detection. The work was sponsored by the Office of Naval Research (ONR) Code 34 Warfighter Performance Department, and was intended to develop a system to be worn by soldiers or other personnel in theater and record and store data associated with explosive blasts that may be related to mild traumatic brain injuries (mTBI). The development effort was a success, culminating in an explosive test resulting in a prototype system gathering data as intended, and those results along with development details are summarized herein.

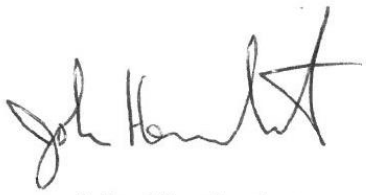

John Hendershot
E3 Division Head

Reviewed by:
Tim Bentley, ONR34, Sponsor
Mike Deeds, E33 Branch Manager, IHEODTD
And All Authors

Approved and released by:
John Hendershot, E3 Division Head, IHEODTD
Kerry Clark, CTO, IHEODTD

This page intentionally left blank.

EXECUTIVE SUMMARY

The ONR Warfighter Performance Department created the Blast Load Assessment Sense and Test (BLAST) Program, which aims to develop a portable, three-part system to measure blast pressure, in order to establish injury thresholds for the brain and analyze potential mTBI causing symptoms. As part of this effort, NSWC IHEODTD was awarded funding from FY15-FY19 to develop a custom low-power soldier-wearable sensing system to detect and store pressure and inertial shock signatures from blast events. Under this effort IHEODTD designed and fabricated custom sensors utilizing micro electromechanical systems (MEMS) technology, assembled them into a custom package containing electronics also designed in-house, and successfully field-tested the entire system under explosive blast conditions. The details of this effort, experimental data collected and conclusions are presented in this report.

This page intentionally left blank.

CONTENTS

Heading *Page*

Tables

Figures

This page intentionally left blank.

ACRONYMS AND ABBREVIATIONS

COTS	Commercial Off-The-Shelf
DRIE	Deep Reactive Ion Etching (Silicon Fabrication)
EOD	Explosive Ordnance Disposal
MEMS	Micro Electro Mechanical Systems
mTBI	Mild Traumatic Brain Injury

This page intentionally left blank.

SECTION 1: INTRODUCTION

1.0 Introduction

ONR initiated the BLAST program in part to "…help recognize the signs of TBI (Traumatic Brain Injury) early and tell warfighters they might need medical attention [1]." The present effort to design a small, accurate and long-battery-life sensing suite is motivated by the Department of Defense's (DoD) desire to assist the large number of personnel who will be exposed to potentially TBI-inducing blasts during the course of their missions. This report outlines NSWC IHEODTD's effort to develop such a sensing suite over the course of 4.5 fiscal years, FY2015 - FY2019. The first 12 pages of this report provide a concise overview of the project with conclusions, followed by subsequent appendices that offer information on technical system development in greater detail.

1.1 Approach

Commercial off-the-shelf (COTS) pressure and inertial (acceleration) sensors are commoditized in consumer electronics markets and are presently inexpensive and relatively precise. However, the majority of these sensors draw power continuously, even when not actively sensing a recordable event, limiting the useful battery life of any portable system built utilizing such sensors. In the present effort, we have combined custom-designed and fabricated sensors that do not draw power continuously – along with custom software – to capture and store data more efficiently than COTS systems, based on electronics that normally sleep and only wake up when a recordable event occurs. Based on this approach, we have built a system with an estimated battery life exceeding 5 years, as opposed to competing systems' reported operational lives of roughly 3 months to 1 year.

1.1.0 Technical Objectives

The main objective of this effort was to iteratively design and demonstrate a system comprising minimally powered (or unpowered) inertial and over-pressure sensors that detect and quantify blast loads capable of potentially inflicting mTBI. The system was required to fit into a compact form factor and store generated data including shock orientation and pressure level with respect to time, to enable future examination by medical professionals. The environmental design parameters cover the pressure and inertial loads potentially capable of causing mTBI, as described in Table 1.

Table 1: Environmental Design Parameters

Parameter	Minimum	Maximum	Minimum Duration	Maximum Duration
Pressure	5 psi	50 psi	0.2 ms	10.0 ms
Acceleration	50 g	250 g	2.0 ms	8.0 ms

1.1.1 Leveraging Experience

In the present effort, IHEODTD leveraged its experience designing MEMS for DoD fuzing applications, involving the safety and reliability of munitions. In addition to sensor design and fabrication experience, the team brought to bear design and testing of custom electronics and associated software required to read, store and transmit sensor data while being supported inside a rapid prototyped enclosure.

[1] https://www.onr.navy.mil/en/media-center/press-releases/2017/onr-blast-tbi-protection

SECTION 2: SYSTEM DESCRIPTION

2.0 System Components

The system comprises a sensor suite with integrated computer processing, data storage, communication and inertial and pressure sensing capability. The initial prototype configuration shown in Figure 1 consists of: two types of sensors; three electronic boards; an internal and external cable; and a soldier-wearable container. The lid of the two-part container, Figure 1(a), carries inertial (b) and pressure (c) sensors mounted on printed circuit boards. The sensor board is connected electrically via ribbon cable (d) to the main electronics board (f) mounted in the body of the container (e). The main electronics board carries a microprocessor for recording and storing data and a micro-USB port for uploading recorded data over a micro-USB cable (g). Figure 2 shows the lid assembly containing a pressure sensor (a) and three orthogonally-oriented inertial sensors (b), with a connector (c) for internal communication. In a design study aimed at reducing system size and testing pressure sensors performance only, a second-generation prototype was designed which didn't contain inertial sensors, and included improved electronics packaging in order to reduce overall volume by 75%, as seen in Figure 3. Additionally, electronics were updated to include a real-time clock chip, enabling accurate time stamps for all events (Figure 4). This tradeoff of smaller volume and reduced system complexity with loss of inertial measurement capability enabled accelerated field testing of larger quantities of pressure sensing systems.

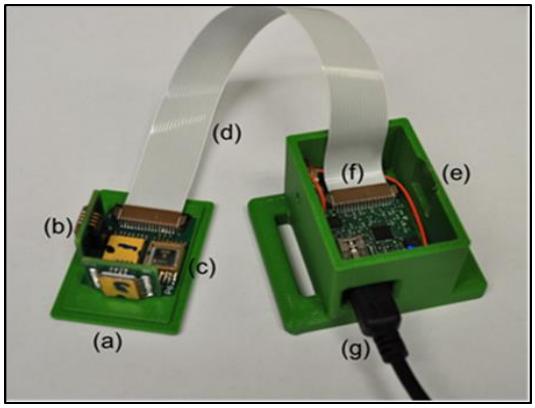

Figure 1: First generation system comprising: sensors (b) and (c), electronics (f), enclosure (a) and (e) and communications cable (g)

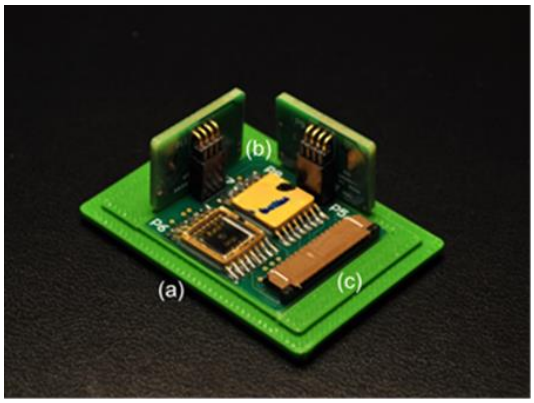

Figure 2: First generation system housing lid, containing one pressure sensor (a), three independent axis inertial sensors (b) and internal connector (c)

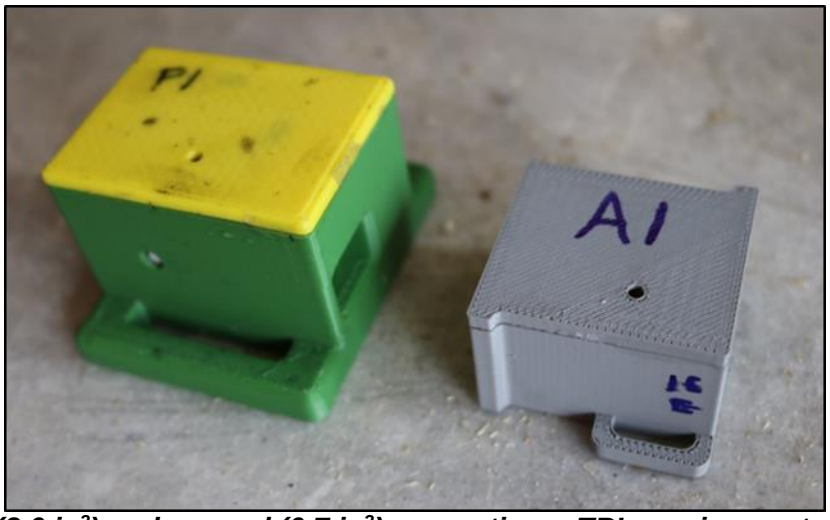

Figure 3: First (3.0 in^3) and second (0.7 in^3) generation mTBI sensing systems, housing all electronics and sensors. A 75% volume reduction was achieved through improved packaging and reduced system complexity, which enabled higher numbers of overpressure field test units

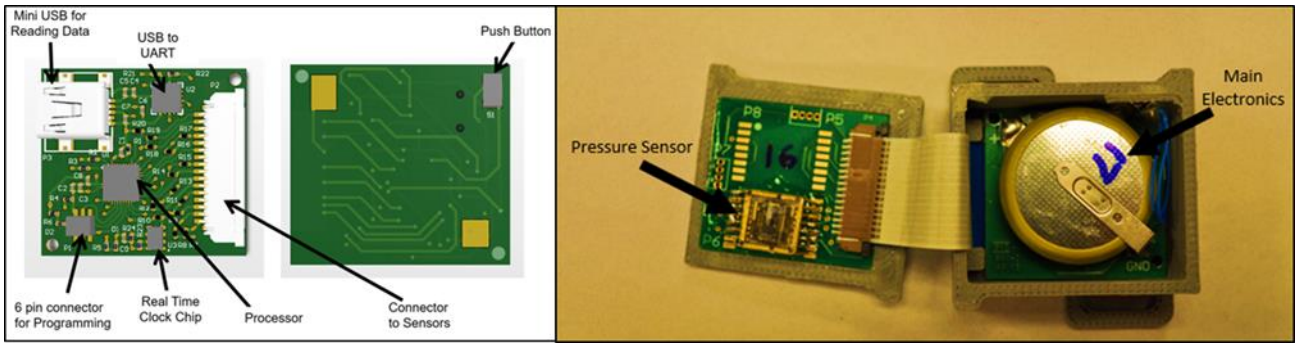

Figure 4: Updated main circuit board and interior view of second generation prototype

2.1 System Operation

The prototype system is designed to attach to clothing utilizing straps via the anchor handles integrated into the container base. When a blast event occurs in close proximity to personnel wearing the present system, the resultant shock wave will impact the sensor suite, creating a response in the inertial and/or pressure sensors, and initiating data recording. Inertial sensors record initial shockwave impact, followed by shrapnel and other subsequent impacts, e.g. the human body coming in contact with its surroundings. The blast overpressure wave impacting the system has a direct path through a port hole in the enclosure lid, seen in Figure 3, to the pressure sensor which saves temporal pressure data to internal memory. All of the readings are recorded on the main electronics board, and can later be downloaded onto a computer via the micro-USB cable.

2.2 Data Processing Utilizing Binned Binary Data Collection

The electronics normally reside in a dormant, low power-consumption state (sleep mode) and are awakened by any of the following four events: pressure rise relative to ambient atmospheric pressure; pressure drop; inertial shock (any axis); or when a data upload is initiated by a user (via transmit button). Upon awakening, the micro-controller (µC) checks transmit button and event history. If a sensor is triggered, a timer is set to zero and every 50 µs the micro-controller checks to see if the sensor changes state. Only upon sensor update does the micro-controller collect its data from the MEMS sensors (through I/O pins) and saves data with a time stamp. This continues for a period of two seconds, at the end of which the current date and time is received from a real time clock chip, all data from this event is saved in flash memory, and the electronics board returns to sleep mode. Alternately, if the data transmit button is activated by a user requesting data upload, all of the data previously saved – that can include multiple events – is transmitted via UART to the computer, via micro-USB cable. See Figure 5 for software logic flow chart.

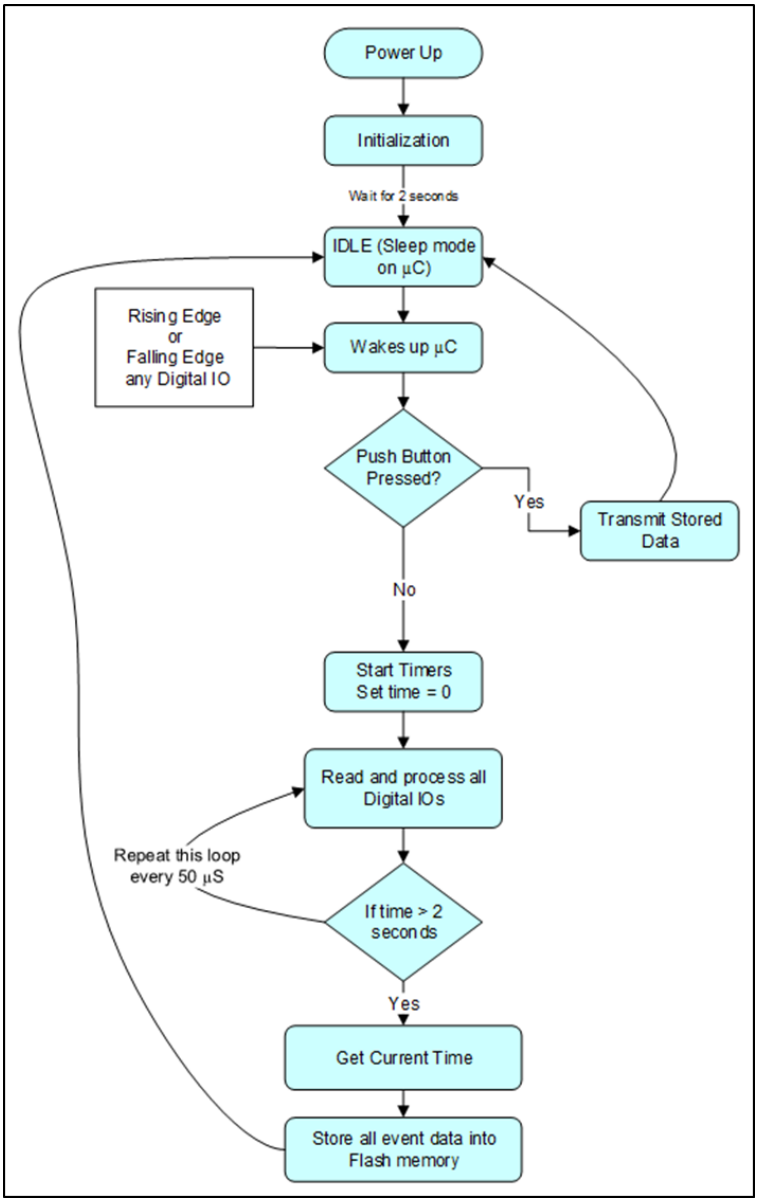

Figure 5: Memory map process flow

In order to extend battery life from less than one year to multiple years, this system was designed to utilize a binary switching and binned data recording approach. This approach greatly reduces the amount of data recorded in a given event, which in turn significantly reduces the required memory space and energy demands on the system. Figure 6 is an example schematic comparing blast pressure data recorded by a COTS reference sensor to a seven sensor-channel custom prototype system from the present effort. A typical sensor system utilizing a continuous time approach would record and store hundreds or thousands of individual data points over each millisecond during an event (depending on the sensor and data collection resolution). The detailed dynamics shown in the reference sensor data are a visual representation of the numerous data points in such a continuous approach, as compared to the approximate 50 data points defining the binned data curves from the prototype system. As seen in this example, there is a data reduction of at least one order of magnitude compared to a typical commercially available system, while still capturing the critical information from the event: namely the peak pressure level and pressure durations.

This approach is realized through the MEMS sensor design described in section 2.3. For example, inside each pressure sensor, individual overhanging conductive silicon cantilever beams contact the conductive silicon pressure membrane at a different pressure threshold and complete individual circuits. This operation represents switches closing at discrete pressures. The system monitors and records each cantilever's circuit, recording the time when that circuit is closed and opened. This results in a data set recorded for each cantilever circuit documenting open/closed time history, representing the corresponding pressure for each cantilever and the time (start and end) of the pressure event. The data from each of the seven cantilever circuits are visualized in Figure 6 as straight line profiles, compared to the continuous reference sensor data. In this example, several of the 10 cantilever circuits were shorted together to utilize less available CPU inputs, resulting in seven total circuits. All seven of the circuits are in contact with the membrane ("switch closed" state) at the onset of the pressure event recorded over 50 psi. The cantilever sensor levels, indicated by their y-axis intercepts, range from roughly 20-50 psi. Each switch closure indicates recorded pressure greater than its threshold value. As the pressure drops below an individual cantilever's pressure threshold, that cantilever loses contact with the membrane and the signal drops to the zero axis on the figure ("switch open" state). As the pressure fluctuates during the blast event, each cantilever continues to record when its threshold is exceeded. The specific COTS reference sensor in this example is a pencil probe (PCB 137B23B) and associated data capture software, which utilizes a quartz sensor in an aluminum body designed for free-field pressures up to 50 psi. This sensor is well characterized, making it a good reference tool for the present effort.

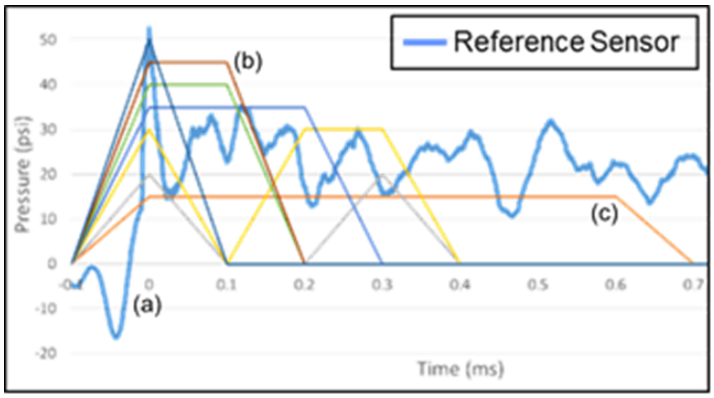

Figure 6: Example of experimental pressure data acquired by prototype sensing system. Seven distinct binned Boolean pressure events were captured (e.g. (b) and (c)), recording essential elements of blast wave profile while requiring significantly less data than COTS continuous pressure measurement reference system (a), also shown for reference.

2.3 Sensors

Two types of sensors microfabricated from silicon are utilized in the present effort: pressure and inertial. The pressure sensing technique used here is patent pending (Navy Case #106,048), and a schematic is shown in Figure 7. The approach leverages an array of microscale cantilever beams to sense multiple binned pressure levels in a single device. The number of cantilever beams utilized determines the resolution of the pressure measurement, and is scalable. A pressure inlet is located on the underside of the lithographically defined conductive membrane. When pressure is applied through the inlet, the membrane deforms upward to form a dome-like shape, represented by the curvature of the membrane in the side profile view of Figure 7. Individual electrically isolated and conductive cantilevers of varying length sequentially contact the membrane on its surface as pressure increases. The longest cantilever makes contact with the membrane first, while shorter cantilevers make contact as the membrane deflects further. At maximum inlet pressure, the membrane is deformed to its maximum height and all overhanging cantilever beams (see Figure 8) are in contact. Contact between beam and membrane is sensed via resistance change, utilizing a common bond pad attached to the membrane and individual cantilever bond pads. These pressure readings are recorded by the system electronics.

A schematic of the inertial sensor is shown in Figure 9. It utilizes an inertial mass with an opposing force defined by two sets of integrated springs ("defined springs" in Figure 9). The mass moves in response to an acceleration event, into a series of contact switches while the springs provide increased resistance proportional to mass displacement. The multi-tiered contact switches indicate acceleration magnitude based upon the number of switches the mass makes contact with (closes). The greater number of switches closed, the greater the acceleration sensed. Individual binned Boolean switch closures are recorded by the system electronics. This type of inertial sensor responds only to acceleration parallel to the long axis of the inertial mass. To sense in three dimensions, one sensor should be placed on each independent orthogonal axis. As fabricated sensors, seen in Figure 10, have a symmetric design allowing movement in either direction on a given axis to be sensed.

The scale of these fabricated prototype sensors is relatively large compared to typical MEMS devices, and they were not optimized for size in this initial development stage. In subsequent development efforts, we believe the overall size can be reduced while retaining functionality.

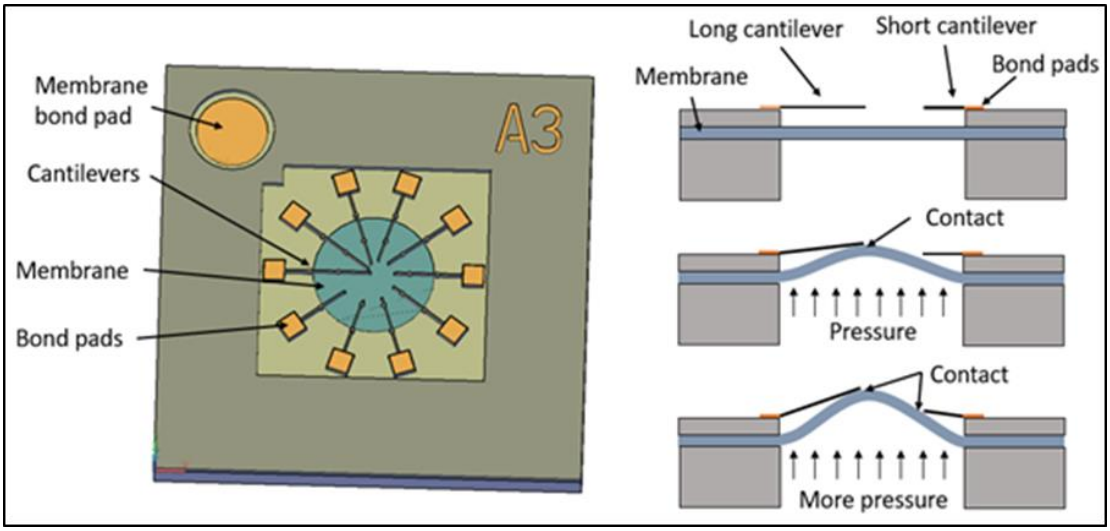

Figure 7: Pressure sensor design schematic shown in isometric view (left) and side profile (right). Conductive silicon cantilevers of varying length overhang an etched conductive silicon membrane. Longer cantilevers are contacted by the conductive membrane initially during deflection, followed by shorter cantilevers at higher pressures. Each cantilever represents a distinct binned Boolean pressure reading.

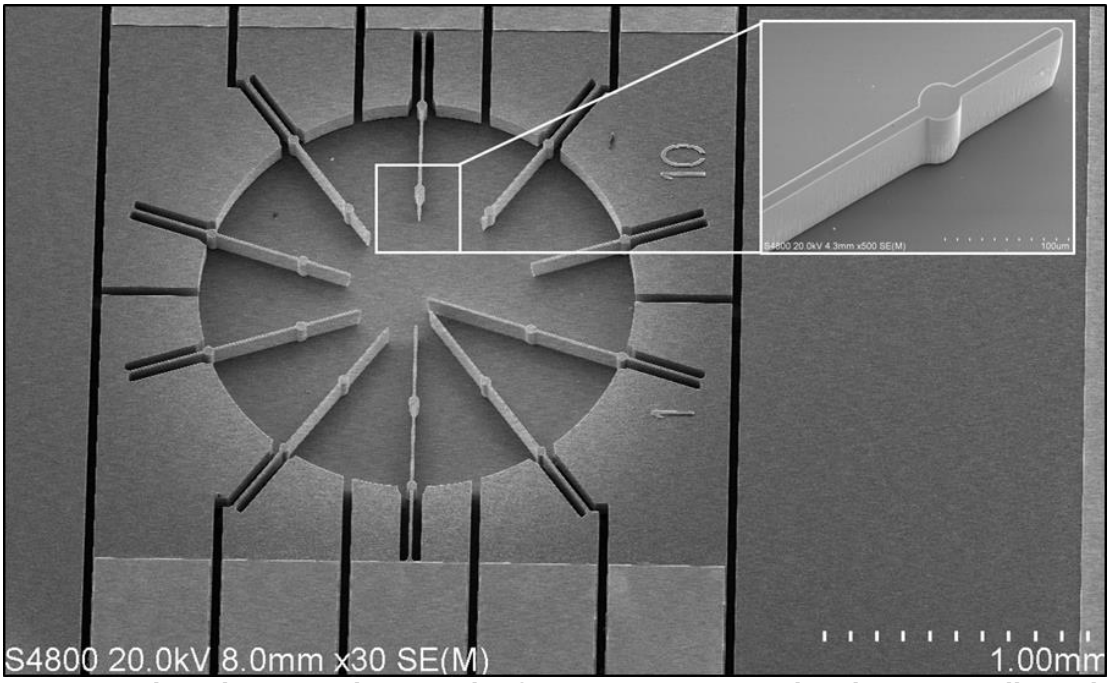

Figure 8: Scanning electron micrograph of pressure sensor, showing 10 cantilever beams overhanging circular diaphragm which deflects in response to pressure

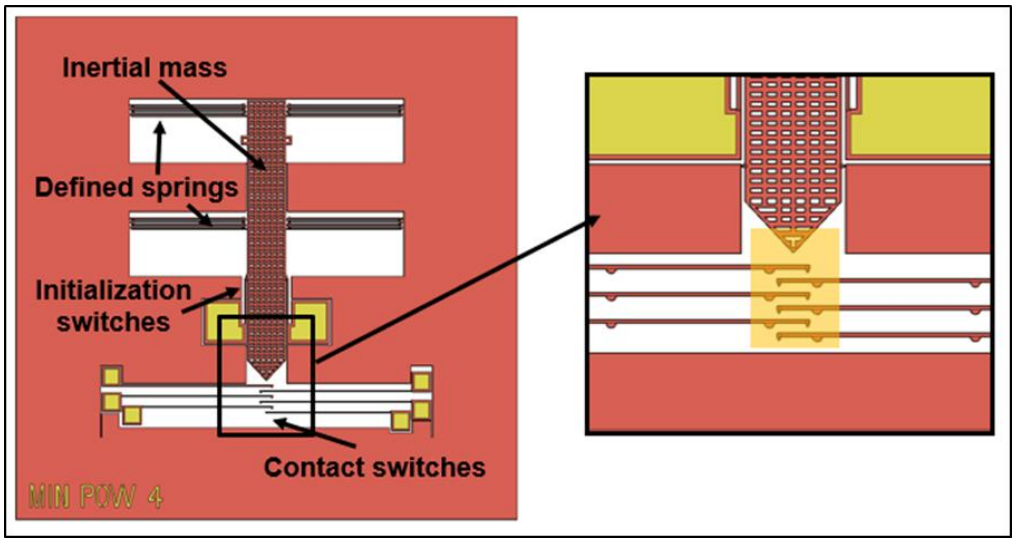

Figure 9: Asymmetric inertial sensor design schematic shown in plan view (left) and detail (right). Increasingly large g-loads lead to conductive inertial mass contact with higher numbers of conductive switches, etched from silicon. In prototype devices, symmetric designs were utilized with bidirectional mass movement and mirrored contact switches on both sides of moving mass.

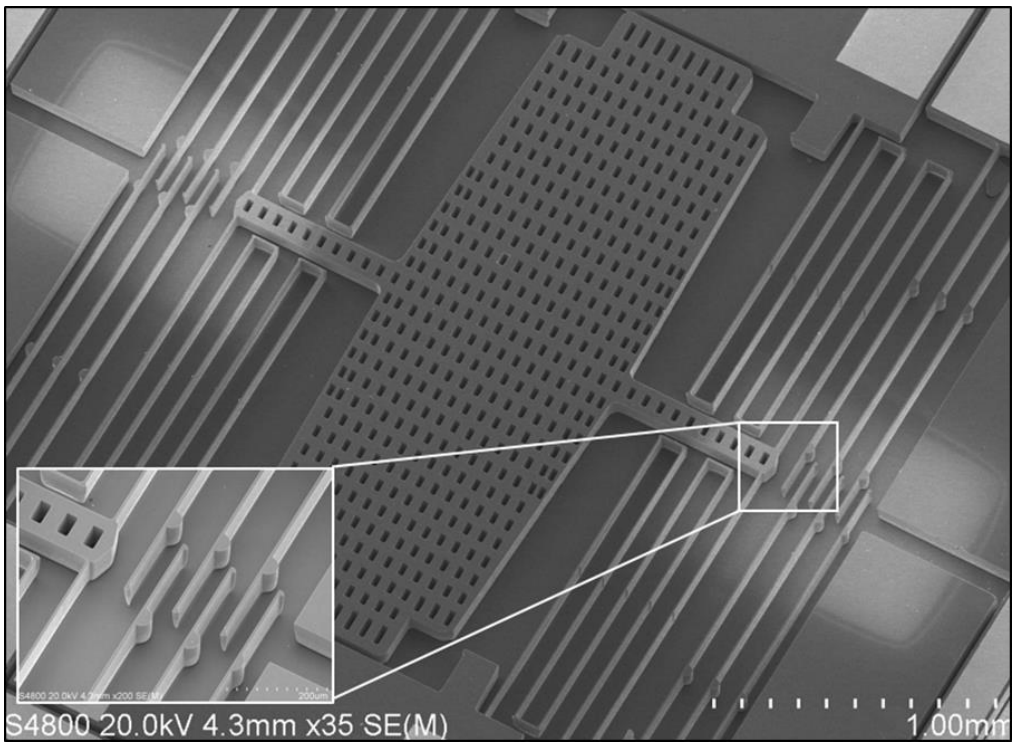

Figure 10: Scanning electron micrograph of inertial sensor, showing large mobile mass in center, flanked on both sides by cantilevered beams that act as switches recording mass movement

SECTION 3: TEST RESULTS

Numerous laboratory tests of individual components, subassemblies and prototype mTBI sensor systems were undertaken before field tests commenced, and some of this background work is described in the appendices of this report. The field tests were the culmination of years of laboratory work, and demonstrated the robustness of the present effort's system realization and overall approach, with respect to sensing and recording pressure sensor data. Due to a desire to increase the number of prototype systems tested and time limitations, pressure-sensor-only systems were field tested (smaller prototype shown in Figure 3).

3.0 Prototype System Field Test Results

In December 2018, a series of explosive field tests was conducted on the present effort's second prototype system, in order to validate it against a real-world blast scenario. The test setup comprised: wooden support structures holding a suspended explosive charge; COTS pressure sensor probes (PCB 137B23B); and mTBI sensor system second prototypes arranged in close proximity to COTS sensors. Sensors were oriented either perpendicular to the direction of incoming explosive shock wave ("reflected pressure") or aligned parallel with the shock wave direction ("incident pressure"), as seen in Figure 11.

The explosive charge and sensors were all stationed 5 feet above ground level. Upon detonation, the explosive fireball extended roughly 5 feet radially from the center of the pentolite charge, and pressure waves were incident on all sensors in each test. In successive tests, the wooden stands holding the sensors were moved closer to the explosive to increase incident pressure. Cast pentolite spheres were chosen as the test explosive due to their well-characterized properties and consistent dimensions; all charges used during testing weighed 600 g ± 1 %. Additional images in Figure 12 show details of both types of mounted sensors utilized in test setup.

In this series of tests, the sensor stands started at 15 feet of radial distance and were moved to within 7 feet from the explosive in a series of five tests, as shown in Table 2. These sensor positions allowed the mTBI system to record pressures that spanned the technical objectives listed in Table 1, with measured pressures ranging from five to 42 psi. Two versions of the MEMS pressure sensor were utilized in this testing, with identical electronics. One version focused on pressures below 10 psi and the another from 8 to 30 psi. The design pressure threshold of each cantilever is specified in the legend of Figure 13 and Figure 14. Both tests utilized identical COTS PCB pencil reference sensors for comparison with mTBI systems. mTBI sensors successfully recorded data in both reflected and incident orientations, and one sample of each orientation is displayed in Figure 13 and Figure 14, respectively.

The results of the high-pressure reflected test are shown in Figure 13. During this explosive event, the initial pressure wave at this particular orientation rose to 30 psi, triggering all five cantilever circuits to close and stay closed for ~0.1 msec, tracking the reference sensor data. During subsequent pressure fluctuations, the 8.5 psi cantilever circuit closed and the 10 and 12 psi circuits were also triggered at 6 and 7 msec, respectively, likely due to reflections. During the low-pressure incident test, shown in Figure 14, the initial overpressure at this particular orientation rose to roughly 12 psi, triggering all five cantilever circuits over their maximum threshold of 8 psi. The overpressure preserved the closed state of all cantilever circuits until the pressure dropped below their threshold, with the exception of the 5 psi circuit that cycled off and on, potentially due to a fabrication anomaly. Once again, there appear to be pressure waves reflected from the environment at 6 and 7 msec, causing four of the cantilever circuits to close again. Overall, these prototype designs of the mTBI system demonstrated good pressure resolution and response time to rising and falling pressures during these tests, in both reflected and incident orientations. During dynamic blast testing, lower pressures were observed to trigger switches that had higher thresholds during static characterization. This relationship is being investigated in an upcoming journal paper.

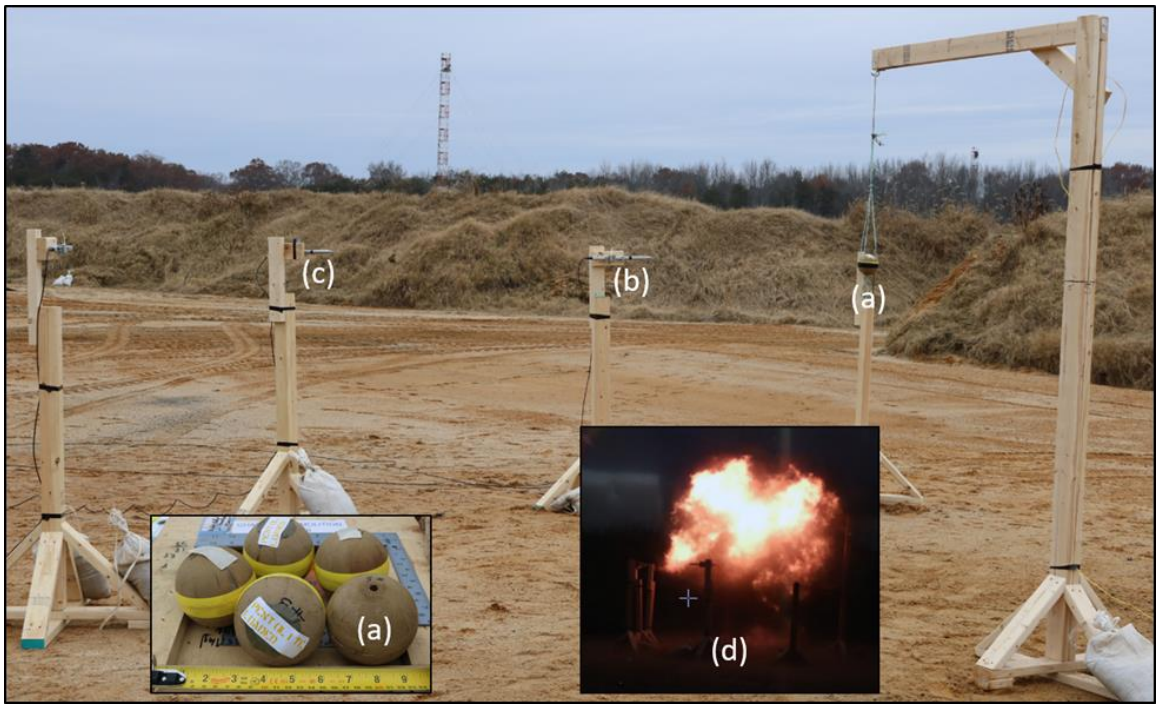

Figure 11: Field test setup comprising: (a) 600 g cast pentolite charge; (b) sensors set up to record reflected pressure; (c) sensors set up to record incident pressure; (d) image of pentolite detonation fireball

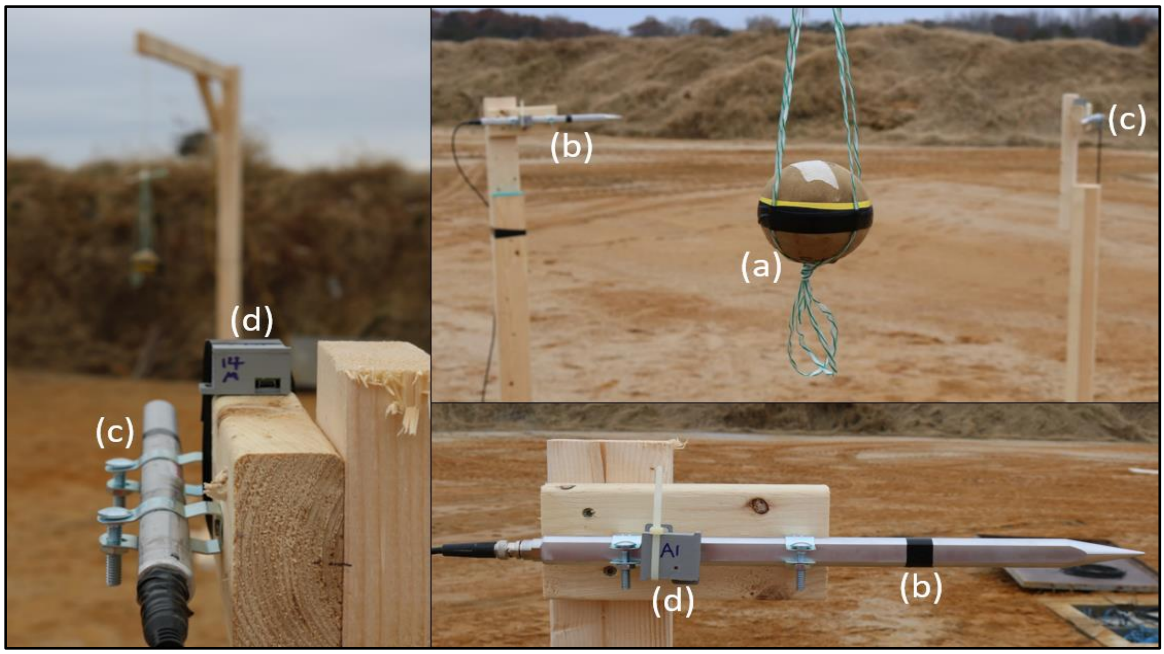

Figure 12: Field test detail images including: (a) 600 g cast pentolite charge; (b) COTS sensor reading reflected pressure; (c) COTS sensor reading incident pressure; (d) mTBI sensor packages under test

Table 2: Maximum reflected and minimum incident blast overpressures recorded at varying radial distances from hanging pentolite charges

Radial Distance from 600g Pentolite Charge [feet]	Minimum Incident Overpressure Recorded [psi]	Maximum Reflected Overpressure Recorded [psi]
15	5	13
11	8	20
9	12	30
8	15	34
7	19	42

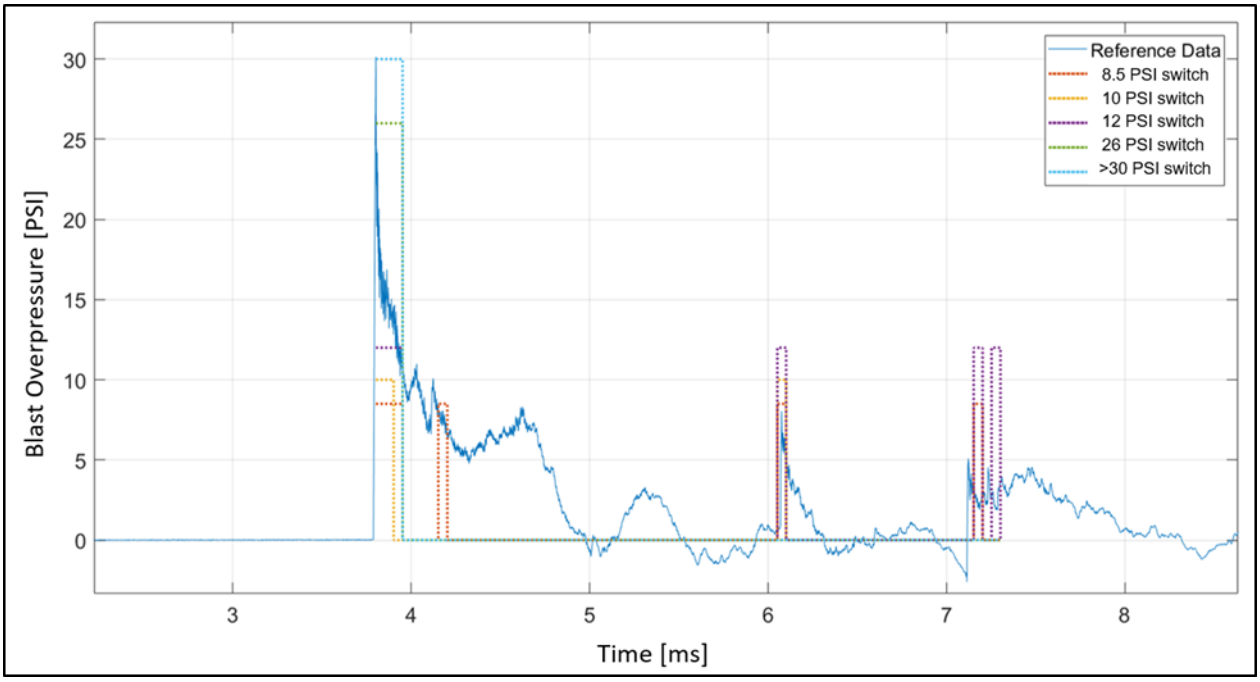

Figure 13: Representative high-pressure reflected experimental results comparing COTS sensor ("Reference Data") and prototype sensor package data, showing good pressure resolution and response time for our prototype system. Our sensor had five internal I/O connections ("switches"), corresponding to between 8.5 psi and over 30 psi during static laboratory calibration testing. Each dotted rectangular bar represents the duration of its respective switch closure; e.g. the highest pressure level switch, calibrated to close over 30 psi during laboratory testing, was activated when the system woke up due to the incoming blast wave, remained high/closed for 100 µs, then went low/open for the remainder of the test, due to subsequent pressure readings staying below 10 psi. Additional pressure pulses, likely due to shock wave reflections from the test environment, were recorded at roughly 6 ms and 7 ms, and our sensor responded to both of these events as well.

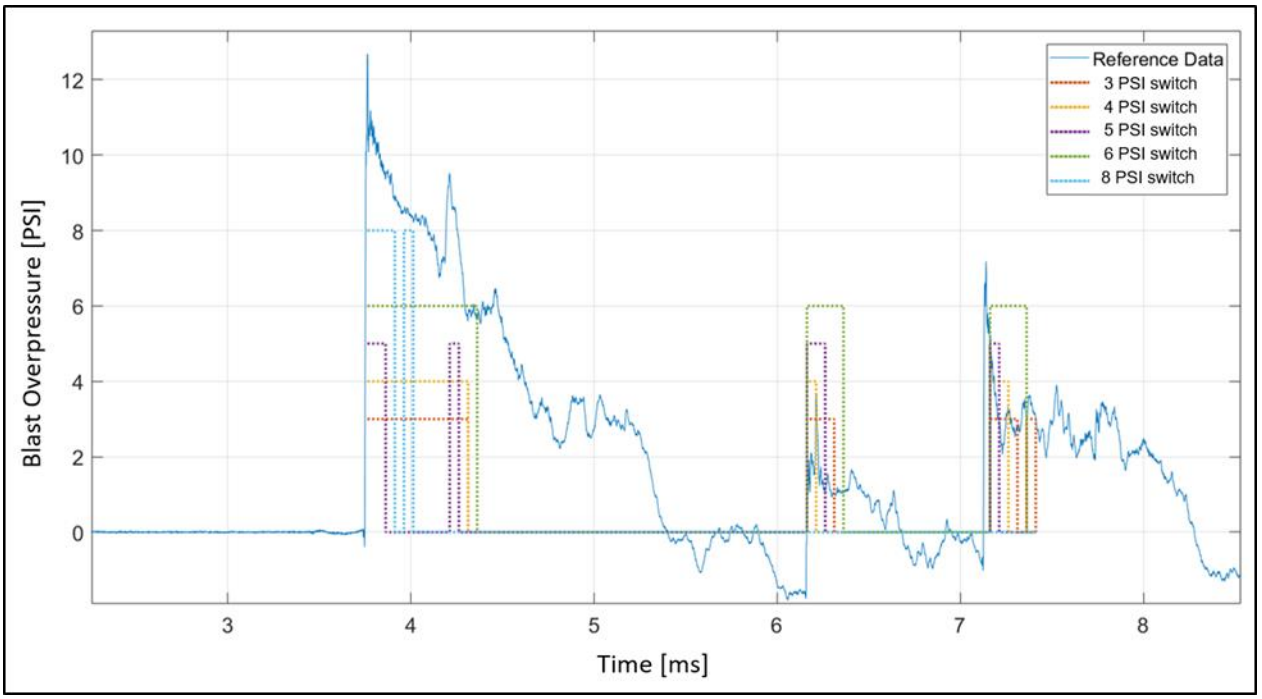

Figure 14: Representative experimental results comparing relatively low-pressure incident blast wave data from COTS sensor ("Reference Data"), and our prototype sensor package, showing good pressure resolution and response time for our system. Our sensor had five internal I/O connections ("switches"), corresponding to between 3 psi and 8 psi during static laboratory calibration. Each dotted rectangular bar represents the duration of its respective switch closure. As the initial pressure pulse is decreasing from its peak over 12 psi back down to 0 psi, the highest pressure switch (calibrated to 8 psi) closes for roughly 100 µs and then opens, while the lower-calibrated switches remain closed for a longer duration, following the behavior of the blast wave. Additional (reflected) pressure pulses were recorded at roughly 6 ms and 7 ms, and our sensor responded quickly and recorded both of these events in addition to the initial event.

SECTION 4: CONCLUSION

NSWC IHEODTD – supported by ONR Code 34 – designed, fabricated, and explosively field tested a soldier-wearable, low-power blast sensing system capable of recording blast events accurately, occupying a volume less than one cubic inch, and with an expected battery life exceeding 5 years. The custom-built prototype system described in this report uses sensors based on MEMS fabrication technology, mated to electronics capable of recording blast events accurately, while leveraging a low-power sleep mode along with a unique data logging approach to enable long battery life. Estimated battery life is years longer than similar previously-fielded systems, with the goal of capturing the key elements of a blast event – namely peak pressure and pulse duration. The system was entirely designed, fabricated and assembled in-house, highlighting IHEODTD's unique capability to prototype custom electro-mechanical systems to meet critical needs. The prototype system was field tested in a blast environment, and demonstrated the capability to accurately record pressure values and quickly respond to dynamic changes in pressure. The prototype system is a good candidate for further development, including reduction of overall system volume, optimization of pressure sensor range/duration, and explosive testing with developed inertial sensors integrated into packaging. Following further development, we hope to transition this technology to an agency that can utilize it to help in the battle against traumatic brain injuries.

This page intentionally left blank.

This page intentionally left blank.

APPENDIX A: MEMS SENSOR DEVELOPMENT

Inertial Sensor Design

During the course of development, we shifted our focus from latching switches that would remain locked in position after an acceleration event, to momentary contact switches that could be utilized multiple times. Switches were also designed symmetrically to allow for bidirectional sensing along a given axis, and die size was reduced from 9 mm square to 6 mm square, to reduce overall package volume. An optical image of both sensors can be seen in Figure 15.

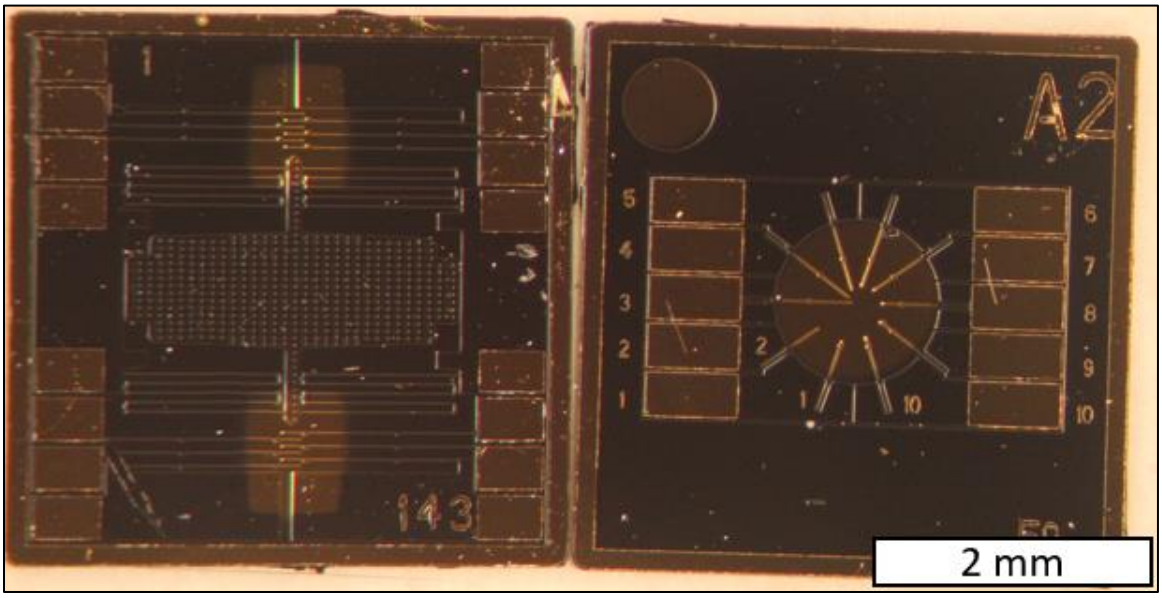

Figure 15: Optical image of inertial and pressure sensor prototype designs

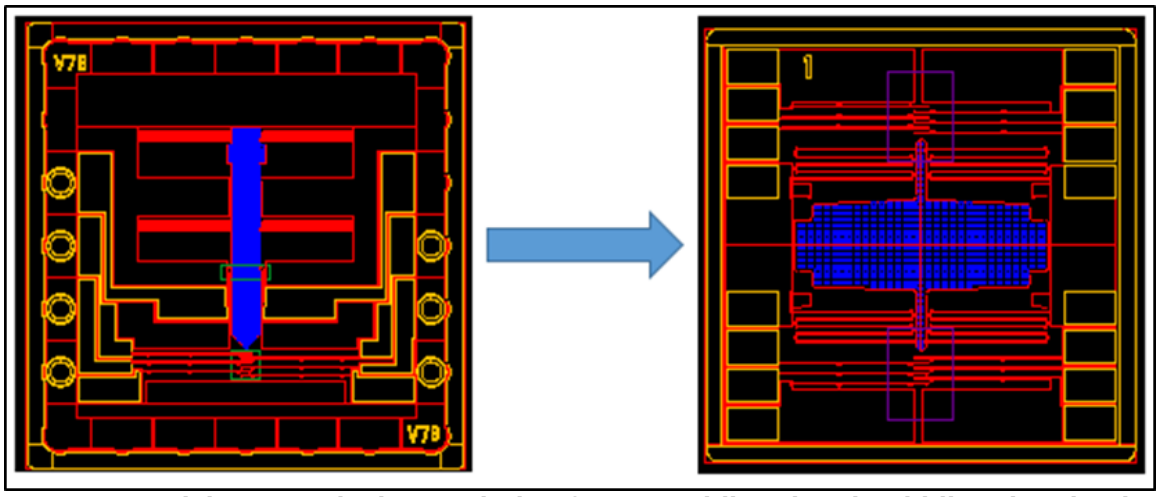

Figure 16: Inertial sensor design evolution from omnidirectional to bidirectional uniaxial sensing

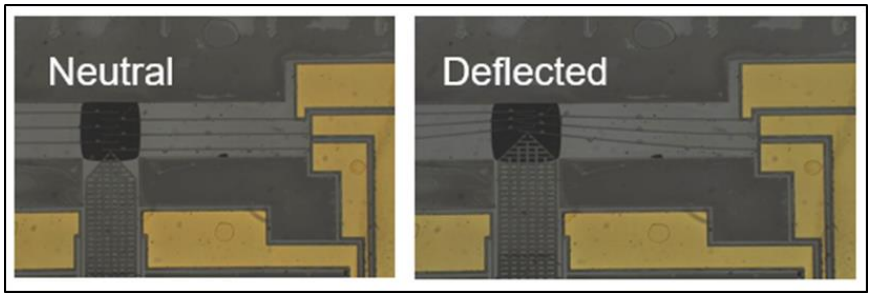

Figure 17: Inertial sensor mass deflection against cantilevered sensing beams

Laboratory shock testing was done using a GHI linear shock table which has programmable shock inputs with adjustable spring preload and hardness of stopper as shown in Figure 18. The shock levels were recorded with an accelerometer, and MEMS sensor outputs were recorded with the data recording. We also constructed a shock sensor model utilizing Matlab Simulink which predicts switch closures from the input accelerometer data.

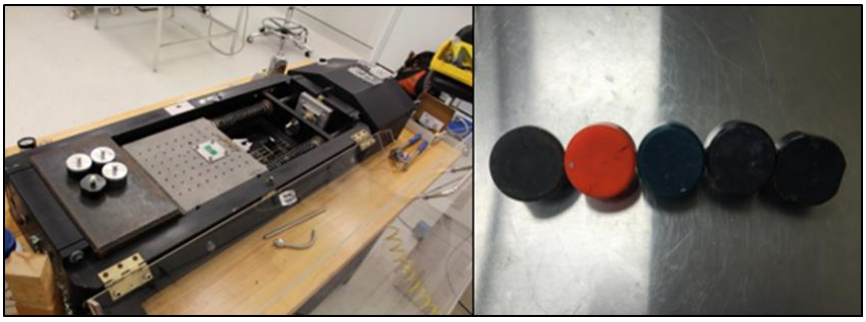

Figure 18: GHI systems linear shock table, together with the programming pucks. These programmers can be interchanged to tune shocks to various levels and durations.

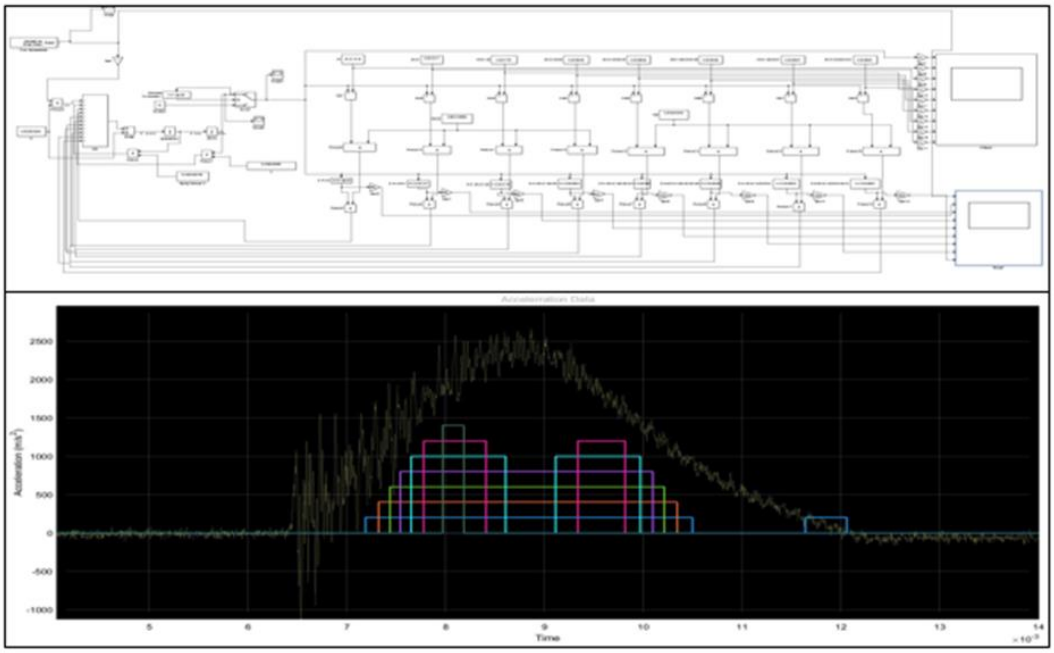

Figure 19: Matlab model of inertial sensor and experimental shock table results

Pressure Sensor Design

Pressure sensor development began with a number of different overhanging sensing beam designs in consideration, including single and double cantilevers, shown in Figure 20. As design progressed, small square contact pad designs were changed to larger rectangular footprint pads, to ease wirebonding. Diaphragm size was varied to enable larger pressure sensing range, and 10 overhanging beams were implemented to give a range of pressure sensing capability within each sensor. Wafer dicing was also eliminated in favor of DRIE etching to singulate chips, which improved manufacturing yield significantly. During static pressure testing of prototype devices, optical profilometry measurements verified expected diaphragm deflections predicted by analytical and numerical modeling (Figure 21). To prepare for field testing, pressure sensors were packaged into chip carriers with epoxy bonding and wirebonded electrical connections.

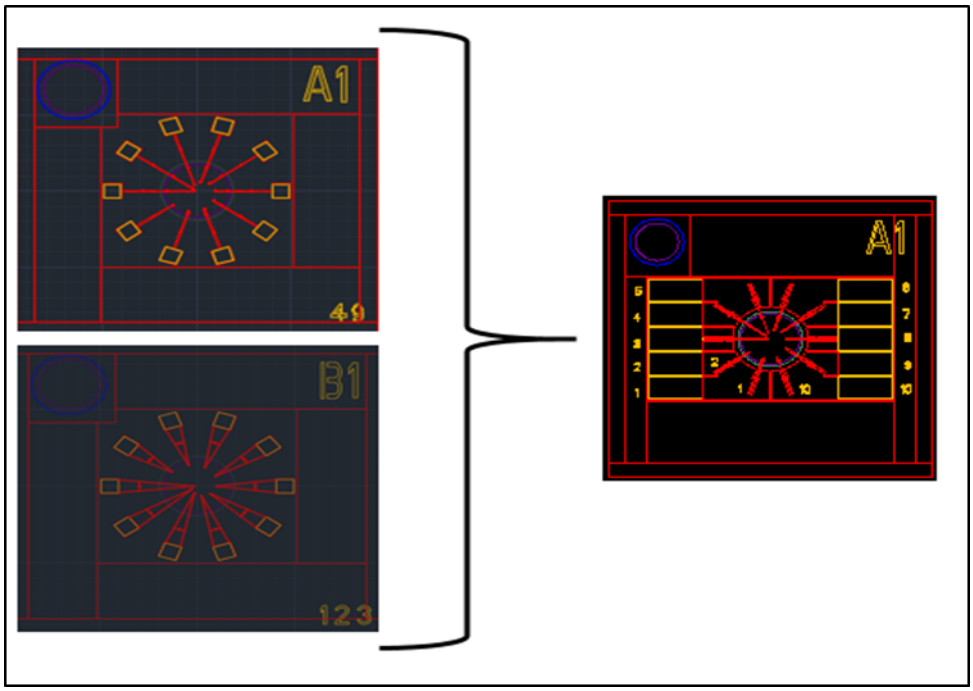

Figure 20: Pressure sensor design progression during project

Figure 21 shows test results from quasi-static testing of pressure sensors. The pressure was applied underneath the diaphragm, causing it to deflect. This deflected diaphragm could be measured with optical profilometery to determine deflection. Pressure was varied utilizing a digital regulator, and switch closures could also be monitored utilizing a multimeter.

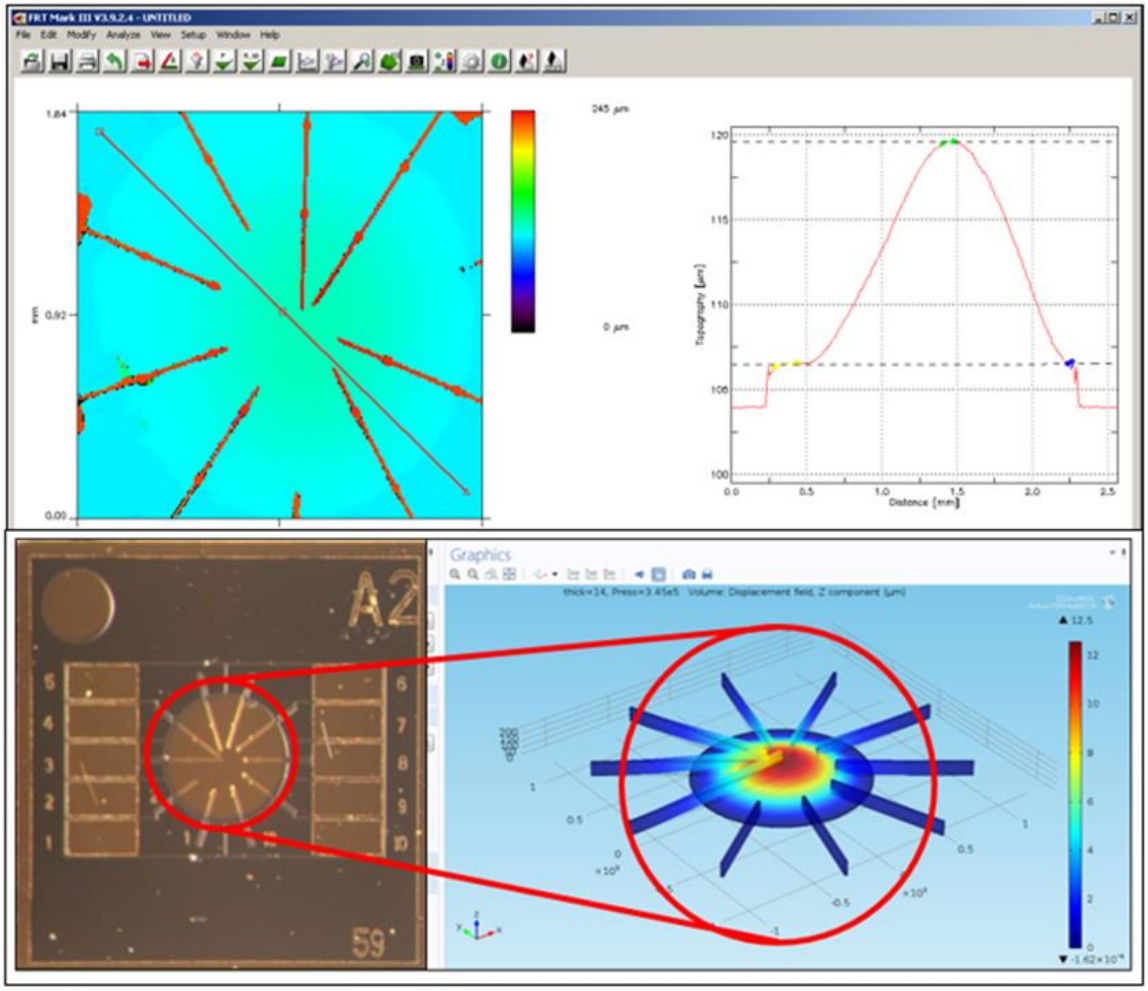

Figure 21: Pressure sensor optical profilometry testing (above) and numerical modeling (below)

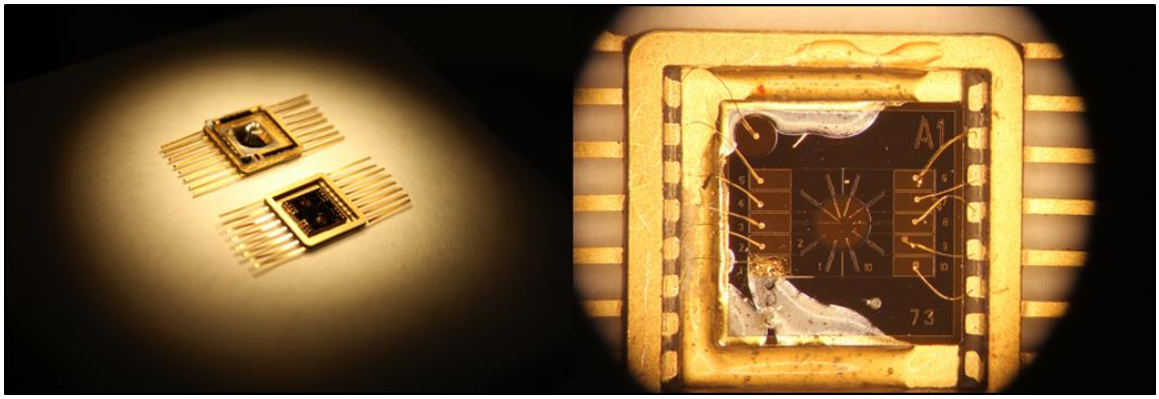

Figure 22: Inertial and pressure sensors packaged inside chip carriers (left); pressure sensor bonded into chip carrier with epoxy and electrically connected via wirebonds (right)

We also collaborated with the Naval Research Laboratory (NRL) (special thanks to Dave Horner and Amit Bagchi) on dynamic lab characterization of prototype pressure sensor designs, with test setups seen in Figure 23. Pressure sensor dies were packaged in chip carriers, with wires extending from the chip carrier to our data acquisition system. The chip carriers were placed inside the shock tube, and shock pulses were incident on the sensor. This data helped us to tune the dynamic range of our sensors.

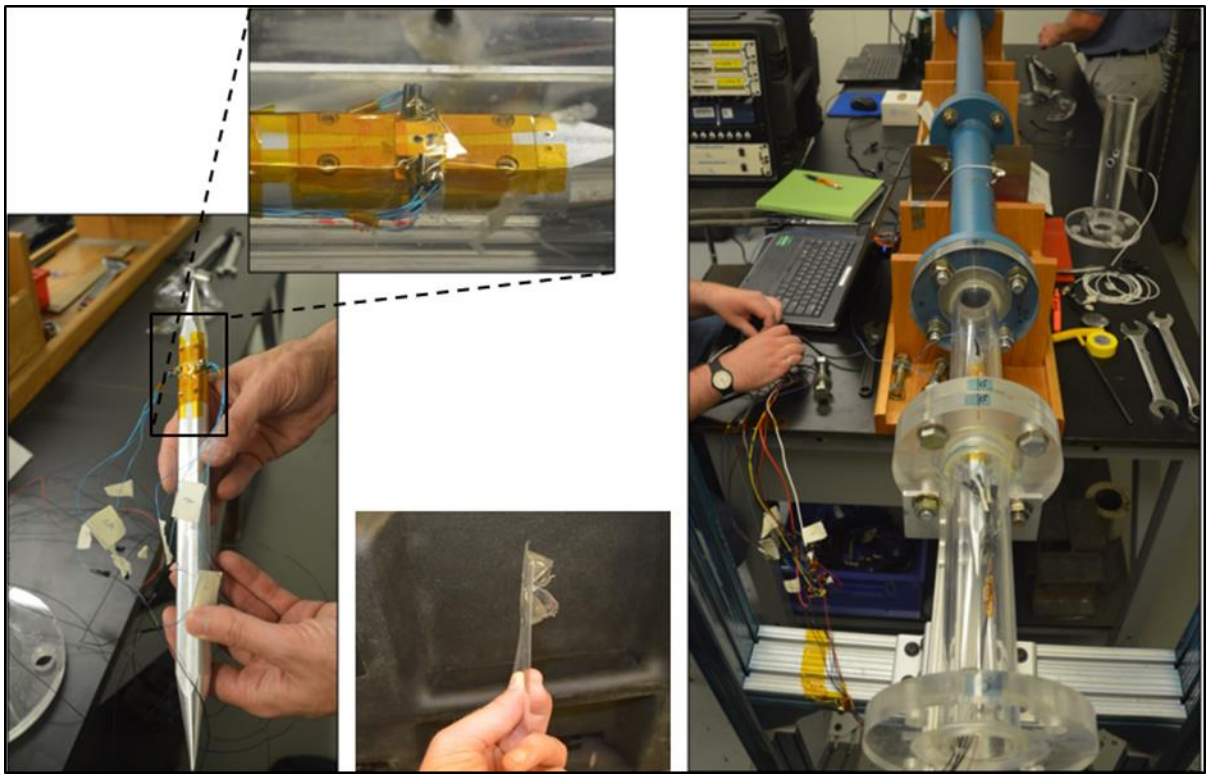

Figure 23: Dynamic pressure sensor testing at NRL utilizing a shock tube. This apparatus applies inert gas pressure on a plastic diaphragm, which ruptures at a known pressure sending a shock pulse traveling down the tube and interacting with a sensor under test. Pressure magnitude and duration can be modified by varying diaphragm material/thickness.

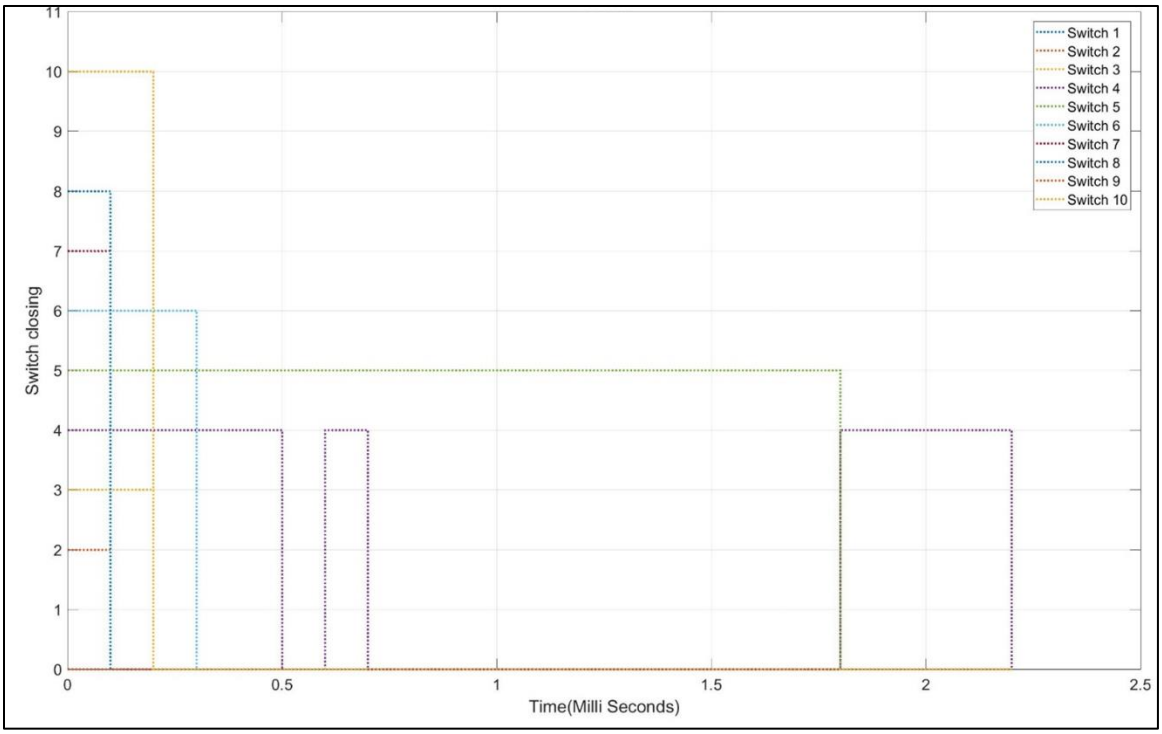

Figure 24: Sample experimental data from NRL dynamic shock tube pressure sensor testing, showing prototype sensor exposed to a 30 psi shock pulse. For a quarter of a millisecond, eight "switches" (individual overhanging cantilever beams) electrically closed their circuits, registering the high initial shock pulse. Subsequently a smaller number of beams, corresponding to lower pressure readings, remained closed as the pressure pulse decreased over time. In this test all 10 overhanging cantilever beams were individually connected to test each of their respective circuits.

APPENDIX B: ELECTRONICS AND SOFTWARE DEVELOPMENT

The goal of the mTBI prototype electronics design is to detect and store MEMS sensor events utilizing minimal power. The MEMS sensors send digital signals to the mTBI electronics indicating which sensor switch is closed. The mTBI electronics read these events from multiple sensors, store them into internal memory, and transfer over micro-USB port upon user request.

Electrical Design

To conserve power, the electronics are designed to stay in sleep mode by default. Upon detecting an event, the electronics wake up for two seconds, continuously monitor the sensors during this two seconds and log changes in sensor output at 50 µs intervals. The microcontroller's internal memory is utilized to store these events. A push button switch is used to initiate transfer of these stored events to an external computer using the integrated micro-USB connection. To minimize total volume of the sensor package, the printed circuit board (PCB) is designed with a goal to fit in 1" x 1" footprint.

The electronics was designed in two major phases. In the first phase it monitored 8 channels and data transfer took place through micro-USB cable (Figure 25).

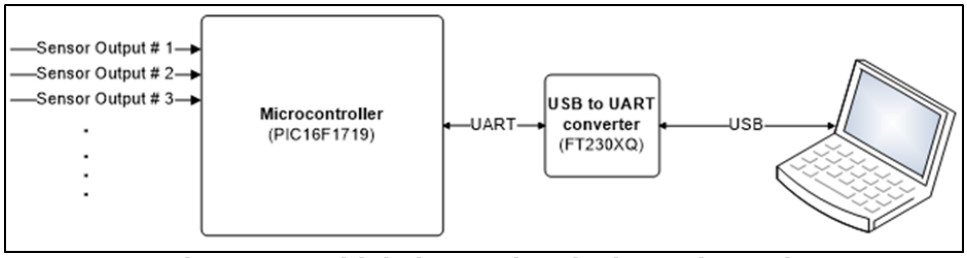

Figure 25: Initial electronics design schematic

In subsequent design evolutions (Figure 26) measurement channels were added, bringing the total to 14 channels (representing 1 MEMS pressure sensor and 3 MEMS inertial sensors) with data transfers takes place using micro-USB. A real time clock chip was also added to give an accurate time stamp through I2C communication. Due to the PIC16F1719 not being able to handle the additional circuitry a new microprocessor was selected (PIC16LF18877). Future work could incorporate wireless data transfer.

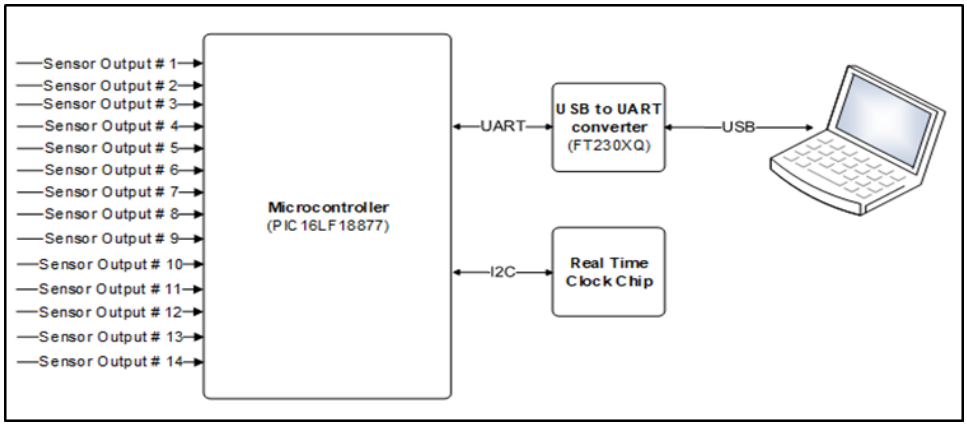

Figure 26: Updated electronics design schematic

Component Selection

The initial electronics design is centered around the 8-bit PIC microcontroller PIC16F1719I/MV. PIC16F1719I/MV chip from Microchip was selected because of its small size (5 mm x 5 mm) and extremely low sleep current of less than 1 µA. In addition, the Microchip has feature rich integrated development environment (IDE) tools, numerous evaluation boards, and online technical support. The following are some major features of this microcontroller:

- 16 MHz internal oscillator block
- Operating Voltage range of 2.3 V to 5.5 V
- 16k words of flash memory
- Minimum sleep current of 50 nA @ 1.8 V, typical
- Minimum Operating Current of 32 µA/MHz @ 1.8 V, typical
- Maximum number of I/O: 35
- Maximum number of A/D channels: 28

The updated electronics design is centered around the 8-bit PIC microcontroller PIC16LF18877I/MV. PIC16LF18877I/MV chip was selected for many of the same reasons as PIC16F1719I/MV. The main reason it was chosen was due to more on chip program memory and twice the total flash memory of the previous chip. The following are some major features of the microcontroller:

- High-precision internal oscillator
    - Software selectable frequency range up to 32 MHz, ±1% typical
- Operating Voltage range of 1.8 V to 3.6 V
- 32k words of flash memory
- 256 B of EEPROM
- Minimum sleep current of 50 nA @ 1.8 V, typical
- Minimum Operating Current of 32 µA/MHz @ 1.8 V, typical
- Maximum number of I/O: 36
- Maximum number of A/D channels: 35

In addition to the microcontroller, a micro-USB to UART converter chip FT230XQ from FTDI is also used to transfer data over the micro-USB port. The chip was selected because of its small size of 4 mm x 4 mm. The chip manufacturer also provides a USB driver software package for this chip. We also added a real-time clock chip AB-RTCMK-32.768KHZ-T3 from Abracon LLC. The chip was selected because of its ease of use instructions, its small size, and its low power capabilities. The following are some of the specs of the chip:

- Operating voltage range of 1.3 to 5.5V
- Current range 0.6 to 4.0 uA
- I2C capable

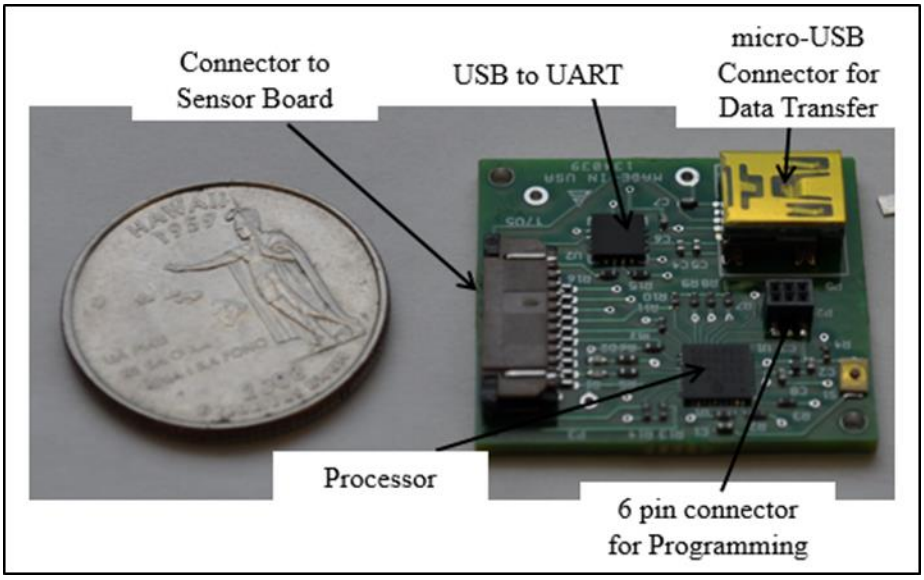

Figure 27: Electronics board shown next to quarter for scale

Schematic

In the first phase of electronics development, the eight channel input schematic with USB driver for data transfer was developed. As described in the block diagram in Figure 28, the microcontroller currently supports up to 19 digital I/O channels with interrupt on change capability. Interrupt on change capability inputs can wake up the microcontroller from sleep upon changing its state from low to high or high to low. The microcontroller also has an additional eight digital I/O channels that do not support interrupt on change feature. A representative schematic is shown in Figure 29.

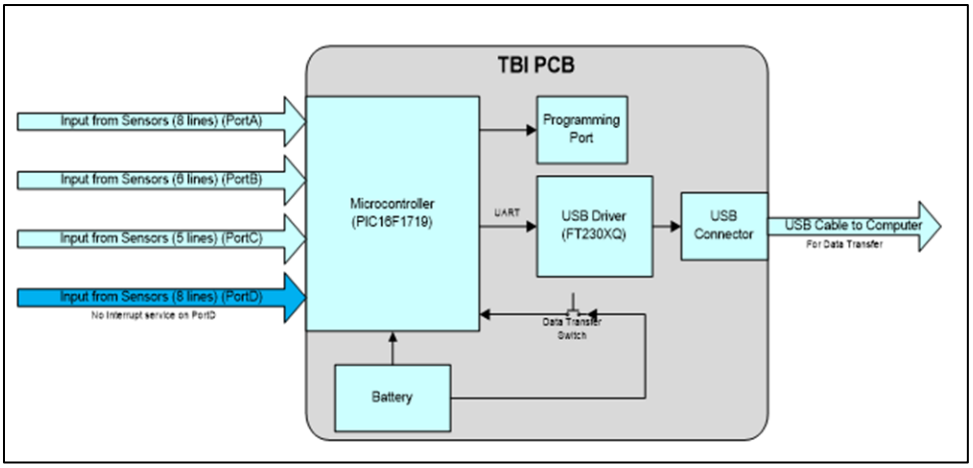

Figure 28: Electronics Design Block Diagram

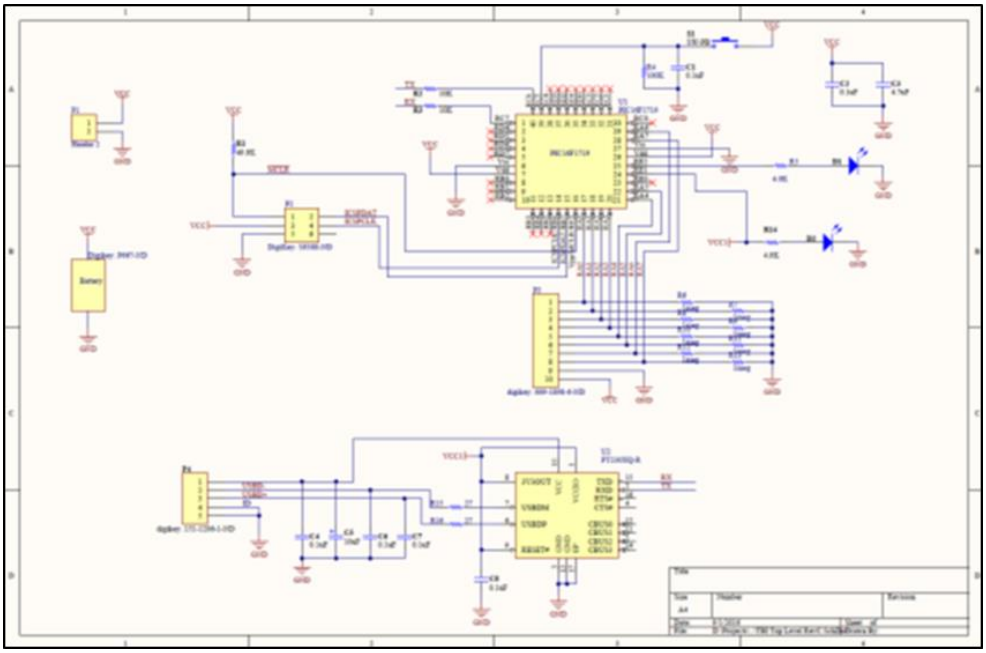

Figure 29: Representative electronic design schematic

Software Design

The software in mTBI is designed to provide a high level of modularity by separating specific functions into separate files. This allows modules to be reused and it allows for a greater level of ease in system debugging.

Software for the mTBI is implemented as a single thread. To reduce the power consumption, the software spends most of the time in sleep (low power) mode. Upon detecting any sensor activity, the microcontroller wakes up by interrupt on event change and starts running in 50 µs loops while collecting data from all sensors. The software collects data for two seconds, and at the end of two seconds it gets the current time and it writes all the readings to internal flash memory and goes back to sleep mode.

Upon waking up from sleep mode, the software checks the digital input pins, and if it detects that data transmission pushbutton is pressed and micro-USB cable is connected, the software executes the data transmission routine. In this routine software reads the data flash memory and transmits previously untransmitted event data to the computer. Figure 30 shows the software flow diagram.

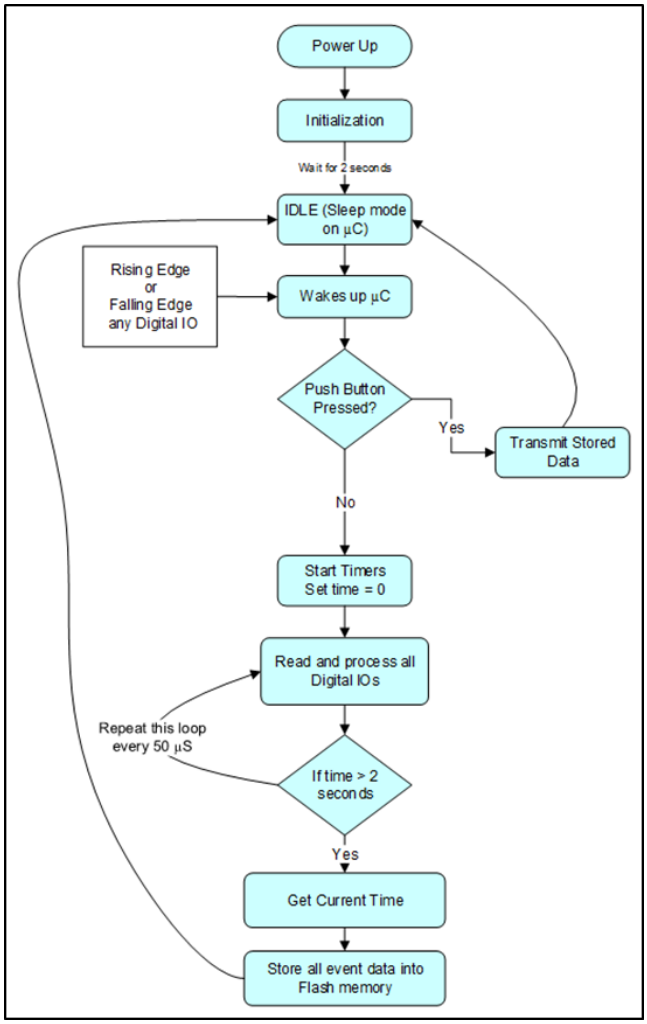

Figure 30: Software flow chart.

```
****************************************************************
  Event ID : 18
  Serial # 6     Event Time: 12/14/18  12:01:31

          Channel Number
         |     Pressure      |    X      |    Y      |    Z      |
 Time(mS) |P1  P2  P3  P4  P5 |X1  X2  X3 |Y1  Y2  Y3 |Z1  Z2  Z3 |
----------------------------------------------------------------------
     0.00: | 1   1   1   1   1 | 0   0   0 | 0   0   0 | 0   0   0 |
     0.15: | 0   1   0   0   0 | 0   0   0 | 0   0   0 | 0   0   0 |
     0.20: | 0   1   1   0   0 | 0   0   0 | 0   0   0 | 0   0   0 |
     0.25: | 0   0   0   0   0 | 0   0   0 | 0   0   0 | 0   0   0 |
```

Figure 31: Example event message on system software user interface

The initial microcontroller selected has a total of 16 kB of internal flash memory. This memory block is partitioned into two blocks: the first 4 kB is used for program memory and later 12 kB are used for data memory. One of the properties of flash memory is that it can be written byte by byte, but it can only be erased in blocks of 32 bytes. During each 2 second time frame, the microcontroller wakes up, runs, and collects data – which is referred to as an "event" in the database. With 12 kB of data memory, the microcontroller could store a total 21 events in its data memory with 60 samples per event. Data memory is further divided into one database header block and 21 event data blocks. The database header takes 1 kB of memory space and each event takes 1 kB of space in memory.

Because of tighter memory space in the microcontroller it is necessary to conserve data space. To reduce number of events stored in memory, the software skips through same repeated readings and stores reading in memory only if any of the input values are changed. As an estimate 60 samples are stored per event, so if inputs change more than 60 times in 2 second event periods, excess readings in the event will be lost and won't get stored. The 60 sample number can be adjusted as needed through the programming, based on requirements derived from test data. Figure 32 shows the memory map of the microcontroller.

Since the microcontroller can only erase flash by row (32 bytes), we are using 32 bytes for each flag in the Database Header section. Table 3 describes the flags used in database header.

Table 3: Database header flag descriptions.

Address	Flag Size	Flag Description
0x1000	1 Byte	0x05 data indicate that the data flash is initialized. Used to detect first time power up of microcontroller.
0x1020	1 Byte	Indicate number of event occurred since last data transfer.
0x1040	1 Byte	Data Read Pointer. Pointer pointing to starting event number that has not been transferred through user interface yet.
0x1060	1 Byte	Data Write Pinter. Pointer pointing to the event number where next event data will be stored.
0x1080	1 Byte	Total number of data events occurred in unit lifetime.

Event Data are stored in data memory as a circular database with first in first out (FIFO). Each event could store date and time stamp for that event. Event data is only erased before writing new data on that event space. At any point in time the microcontroller has its last 21 event data stored in its memory. Once it reaches max number of events, the database pointer rolls back and start overwriting oldest data, which is beginning of database. Table 4 describes flags and data used in each event.

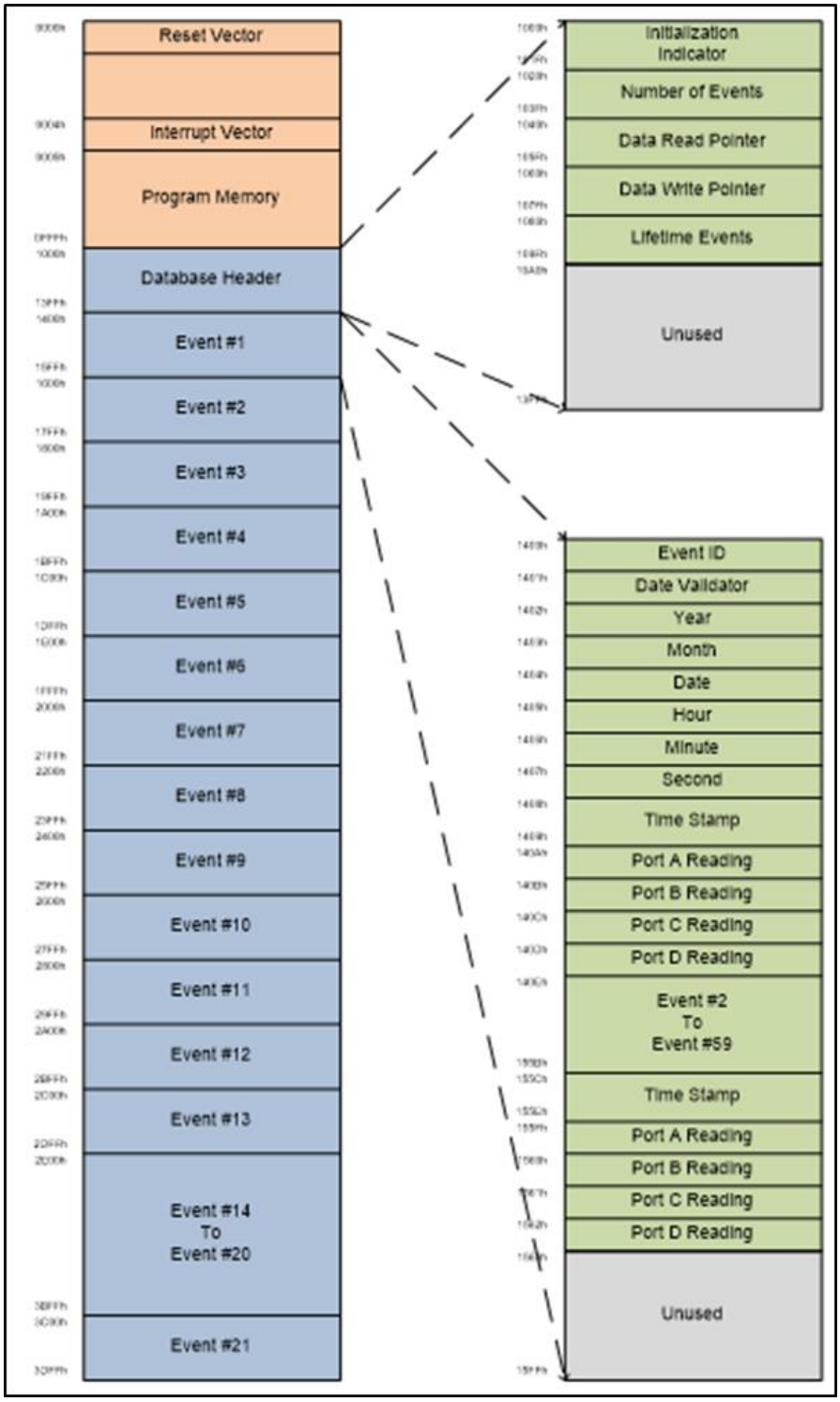

Figure 32: Microcontroller memory map

Table 4: Flags and data utilized during event capture.

Address	Flag Size	Flag Description
0x1400 - 0x17FF	1K Byte	Event Number - 1, max 60 readings
0x1400	1 Byte	Event ID; microcontroller is storing 21 events so this number will be between 01 to 21.
0x1401	1 Byte	Valid data indicator; microcontroller write 0x2A at the end of event data writing cycle so this number indicate that full event data writing in the memory is successful.
0x1402	1 Byte	Two digit Year (YY) (not implemented yet)
0x1403	1 Byte	Two digit Month (MM) (not implemented yet)
0x1404	1 Byte	Two digit Date (DD) (not implemented yet)
0x1405	1 Byte	Two digit Hour (HH) (not implemented yet)
0x1406	1 Byte	Two digit Minute (MM) (not implemented yet)
0x1407	1 Byte	Two digit Second (SS) (not implemented yet))
0x1408 - 0x140D	6 Byte	Reading Number - 1
0x1408	2 Byte	2 Byte relative time stamp. Number of 100 microseconds from start of an event.
0x140A	1 Byte	Port A reading
0x140B	1 Byte	Port B reading (not implemented)
0x140C	1 Byte	Port C reading (not implemented)
0x140D	1 Byte	Port D reading (not implemented)
0x140E - 0x1413	6 Byte	Reading Number - 2
...		...
0x155B - 0x1563B	6 Byte	Reading Number - 60
0x1600 - 0x17FF	0.5K Byte	Event Number - 2, max 60 readings
...		...
0x3C00 - 0x3DFF	0.5K Byte	Event Number - 21, max 60 readings

The updated microcontroller has a total of 32 kB of internal flash memory, though we currently only use 29 kB. This memory block is partitioned into two blocks, first 8 kB is used for program memory and later 21 kB are used for data memory. One of the properties of flash memory is that it can be written byte by byte, but it can only be erased in blocks of 32 bytes. Each 2 second time frame microcontroller wakes up, runs, and collects data is referred to as an "event" in the database. With 21 kB of data memory, the microcontroller could store a total 40 events in its data memory with 60 samples per event. One of the major differences between the two microcontrollers is this one contains an EEPROM to act as the database header. since EEPROM is erased and written word by word (rather than line by line) and that it is considered a separate memory location, allowing more room to store “event” data.

In order to reduce the number of events stored in memory, the software skips through identical repeated readings and stores reading in memory only if any of the input values have changed. As an estimate 60 samples are stored per event. That means if inputs changes more than 60 times in a 2 second event period, excess readings in the event will be lost and won't get stored. The 60 sample number can be adjusted as needed through the programming, based on requirements derived from test data. Figure 32 shows the updated memory map of the microcontroller.

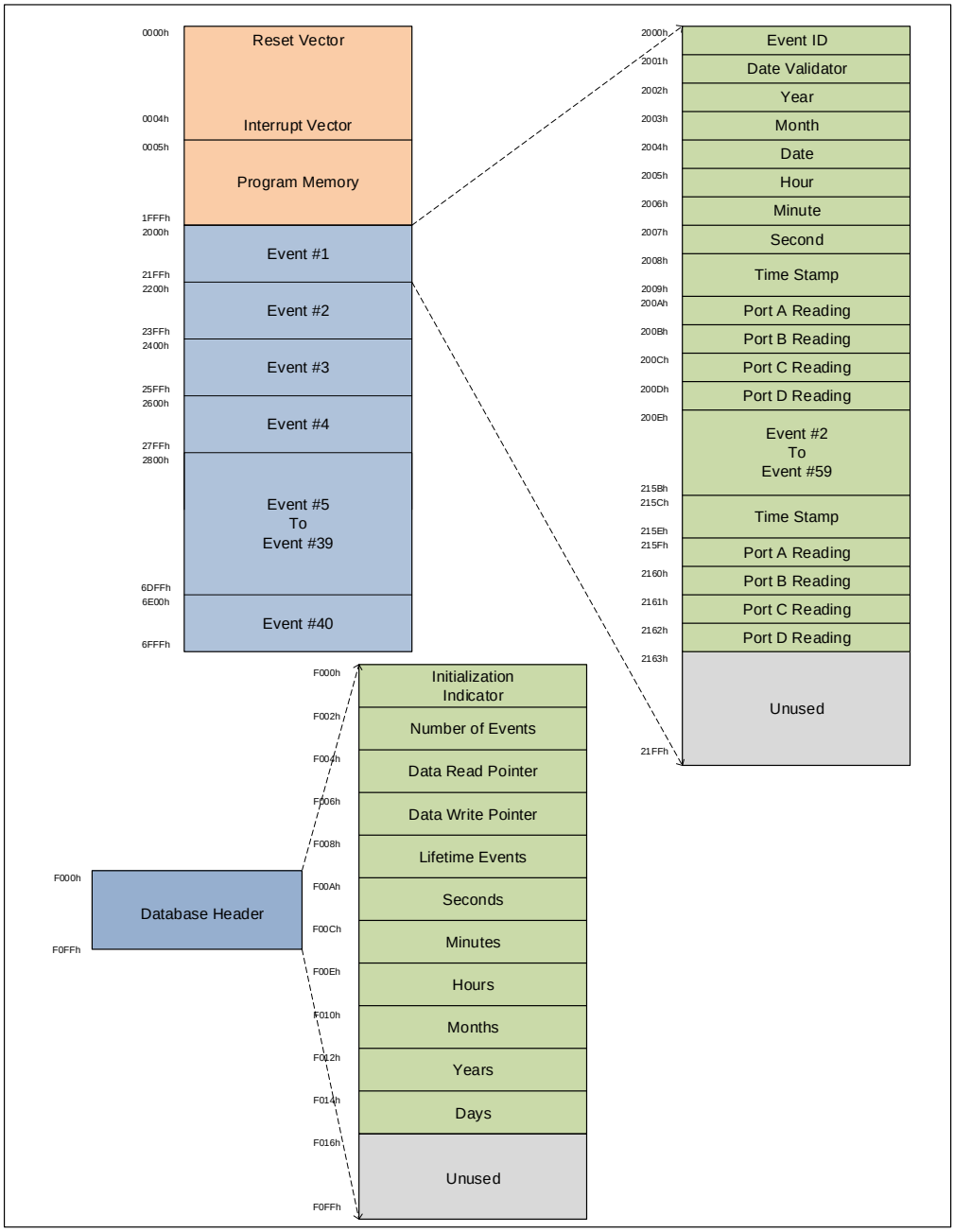

Figure 33: Updated memory map

Table 5: Database header flag descriptions.

Address	Flag Size	Flag Description
0xF000	1 Byte	0x05 data indicate that the data flash is initialized. Used to detect first time power up of microcontroller.
0xF002	1 Byte	Indicate number of event occurred since last data transfer
0xF004	1 Byte	Data Read Pointer. Pointer pointing to starting event number that has not been transferred through user interface yet.
0xF006	1 Byte	Data Write Pointer. Pointer pointing to the event number where next event data will be stored.
0xF008	1 Byte	Total number of data events occurred in unit lifetime.
0xF00A	1 Byte	Seconds: Current Second from timer chip
0xF00C	1 Byte	Minutes: Current Minute from timer chip
0xF00E	1 Byte	Hours: Current Hours from timer chip
0xF010	1 Byte	Months: Current Month from timer chip
0xF012	1 Byte	Years: Current Year from timer chip
0xF014	1 Byte	Day: Current Day from timer chip

Event data are stored in data memory as a circular database with FIFO. Each event can also store date and time stamp for that event. Event data is only erased before writing new data set on that event space. That means at any point of time a microcontroller has the last 40 event data stored in its memory. Once it reaches its max number of events, the database pointer rolls back and start overwriting the oldest data, which is located at the beginning of database. Table 6 describes flags and data used in each event.

Table 6: Flags and data utilized in event recording.

Address	Flag Size	Flag Description
0x2000 - 0x21FFh	1K Byte	Event Number - 1, max 60 readings
0x2000	1 Byte	Event ID; microcontroller is storing 40 events so this number will be between 01 to 40.
0x2001	1 Byte	Valid data indicator; microcontroller write 0x2A at the end of event data writing cycle so this number indicate that full event data writing in the memory is successful.
0x2002	1 Byte	Two digit Year (YY)
0x2003	1 Byte	Two digit Month (MM)
0x2004	1 Byte	Two digit Date (DD)
0x2005	1 Byte	Two digit Hour (HH)
0x2006	1 Byte	Two digit Minute (MM)
0x2007	1 Byte	Two digit Second (SS)

0x2008 - 0x200D	6 Byte	Reading Number - 1
0x2008	2 Byte	2 Byte relative time stamp. Number of 100 microseconds from start of an event.
0x200A	1 Byte	Port A reading
0x200B	1 Byte	Port B reading (not implemented)
0x200C	1 Byte	Port C reading (not implemented)
0x200D	1 Byte	Port D reading (not implemented)
0x200E - 0x2013	6 Byte	Reading Number - 2
...		...
0x215B - 0x2563	6 Byte	Reading Number - 60
0x2200 - 0x23FF	0.5K Byte	Event Number - 2, max 60 readings
...		...
0x6E00 - 0x6FFF	0.5K Byte	Event Number - 21, max 60 readings

User Interface

A USB bus is used to transfer data from the microcontroller's internal memory to the user interface. Data transfer can be initiated by pressing the "Data Transfer" pushbutton on the PCB. This pushbutton wakes up the microcontroller from sleep mode. Once the software wakes up it checks that pushbutton is activated then it verifies that micro-USB cable is plugged in and if both conditions are met, the software initiates data transmission from the microcontroller's internal memory. The microcontroller transmits previously un-transmitted event data from its memory. The microcontroller transmits these data over its UART bus and an UART to USB convert chip converts these data into USB and transmits it to the computer. Putty or any other serial terminal software is used with the following settings to receive data from electronics. An example output image was shown in Figure 31.

- Baud Rate: 115200
- Data bits: 8
- Parity: None
- Stop bits: 1
- Flow Control: None

Battery Life

Two battery options were investigated for powering the data logging electronics. Measurements of the actual power draw of the electronics were made in order to estimate battery life and thus service life of the device: 1.86 mA when awake, and 0.01 mA when asleep, at 3 V. A commercially-available lithium 3 V coin cell (CR2477) was chosen for maximum energy per volume. The lifetime calculation assumes 20 recorded events per day, with 2 seconds per recording. Table 7 and Figure 34 show the details of the two battery options traded during prototyping.

Table 7: Two batteries traded during prototyping

Battery	Capacity (mAh)	Size	Days	Years
Panasonic BR2330	255	23 mm x 3 mm, 3.2 grams	685	1.88
Panasonic CR2477	1000	24.5 mm x 7.7 mm, 10.5 grams	2,687	7.36

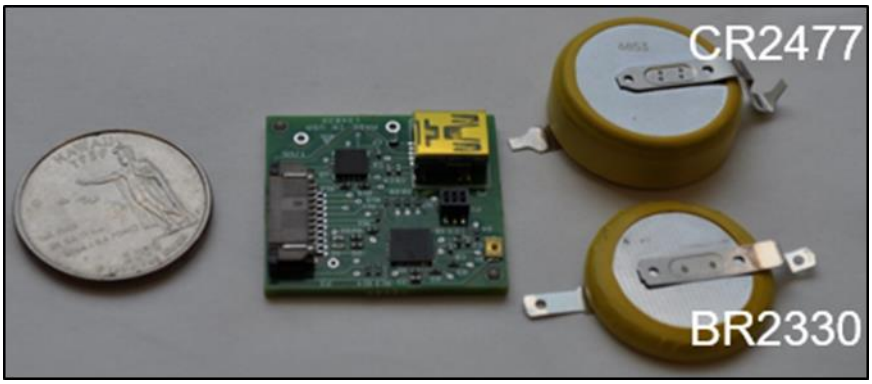

Figure 34: Two batteries traded during prototyping, with US quarter for scale. CR2477 was selected to maximize system battery life.

APPENDIX C: BETAVOLTAIC (NON-CHEMICAL) MICRO-POWER SOURCES FOR MEMS SENSING APPLICATIONS DEVELOPMENT

Objective

The purpose of this sub-effort was to investigate micro-scale power sources for the mTBI blast sensing system that were smaller in size than conventional batteries and also did not rely on stored chemical energy. The goal was to research and potentially develop either: a power supply based on a betavoltaic microbattery that could power the system completely; or alternately to develop a system designed to re-charge the existing battery during sleep mode, in order to extend its lifetime past 10 years of service life. This development work did not culminate in a betavoltaic source powering a prototype in the present effort, but laid the ground work for future follow-on efforts. Based on our work in this area, we feel that these types of sources are good candidates to power future low-power sensors.

Introduction

Betavoltaic devices are long life (>10 years) power sources which convert nuclear energy released as ionizing radiation (beta particles) directly into electrical energy, and have at least 100 times the energy density of state of the art chemical batteries. The power generated by these devices is low (nano-Watts to micro-Watts) but they provide a constant power source which is very small (millimeter scale or below) and can function in extreme environments (under water, abnormal heat/cold). A betavoltaic device has two major components: a semiconductor junction in the form of a p-n/p-i-n diode and a beta source such as Nickel-63 as shown in Figure 35.

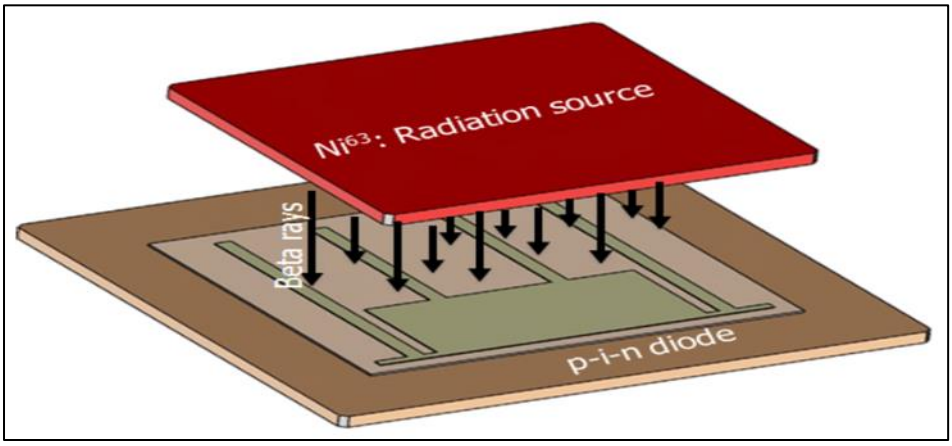

Figure 35: Betavoltaic Power Source Schematic

The working principle of a betavoltaic device is similar to a solar cell, but instead of electron hole pairs (EHPs) being generated by photons, they are generated by beta particles. Because beta-sources have long half-lives, high energy density (orders of magnitude more than chemical batteries), and are insensitive to temperature variations, they are well suited for applications such as electronics for wearable technology or sensors in remote locations. Tritium (^{3}H) and Nickel-63 (^{63}Ni) are two of the common beta sources used for betavoltaic devices and are commercially used in exit signs and on watches hands.

Brief Literature Review

The electron (beta)-voltaic effect was first reported by Ehrenberg in 1951 when he observed that a selenium photocell was sensitive to electrons when bombarded with an electron beam [1]. In 1953, Paul Rapport suggested the use of a p-n diode for the conversion of beta radiation into electrical energy and his experiment yielded an

efficiency of 0.4% [2]. During the period between the 1960s through the 1990s, numerous laboratories extensively developed and tested betavoltaic devices, especially Donald W. Douglas laboratories (1968-1974). A device, the Beta-Cell model 400, showed an overall efficiency of approximately 1.7 % by using promethium-147 (half-life 2.6 years) as a beta emitter. It was also applied to a cardiac pacemaker, which was expected to last for 10 years [3]. From the investigations during that period, the overall efficiencies of the devices were poor, and researchers also found that high energy beta radiation caused significant damage to the rectifying junction, thus degrading the performance and shortening the lifetime of betavoltaic devices.

Since the 1990s, researchers have investigated different ways to improve the performance of betavoltaic devices. In order to reduce the radiation damage to the rectifying junction, highly radiation tolerant materials such as silicon carbide (SiC) were explored. In 2006, a SiC p-i-n junction betavoltaic cell was fabricated using chemical vapor deposition on a low resistivity n-type 4H-SiC substrate and tested with phosphorus-33 (^{33}P). It produced a conversion efficiency of ~4.5% [4]. The device had an output power density of 2.1 μW cm^{-2} and no device degradation effect was observed over 3 months (four half-lives of the beta source) [4]. In the same year, Chandrasekhar investigated a 4H-SiC p-n structure under the ^{63}Ni source and obtained an overall efficiency of ~6% [5]. However, the output power of the device was very low (current density of 16.8 nA cm^{-2} and open circuit voltage of 0.72 V) [5]. Despite these improvements, the basic structure of betavoltaic cells have remained constant since their discovery almost 67 years ago, but the maximum efficiencies have only reached approximately 6 %.

The output power of a betavoltaic device increases with the increase of the energy gap (Eg) of a semiconductor material as shown in Figure 36 [6]. Compared with Si (Eg = 1.12 eV) and 4H-SiC (Eg = 3.21 eV), the wider energy bandgap of gallium nitride (GaN) with Eg =3.4 eV is a more attractive choice for producing a betavoltaic device [6].

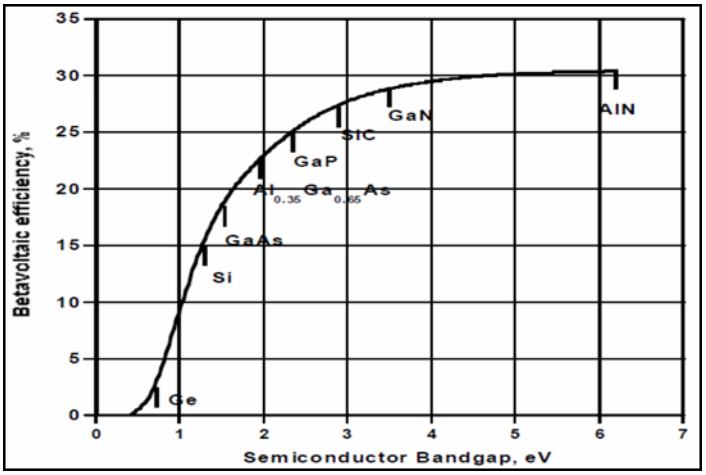

Figure 36: Theoretical device efficiency as a function of material band gap energy.

Fabrication and Characterization of Prototypes

We fabricated betavoltaic devices on GaN in a p-i-n structure. The structure was commercially purchased, however the epitaxial layers were customized according to our specifications, as shown in Figure 37. The i (intrinsic) layer in the middle of a p-n junction is used to increase the depletion region (collection area of carriers) width, resulting in better efficiency and increased output power. The betavoltaic devices were designed similar to solar cell structures due to similarity in working principle, as both require a p-n diode structure. Betavoltaic device design is shown in Figure 38, and an optical image of a fabricated device is shown in Figure 39.

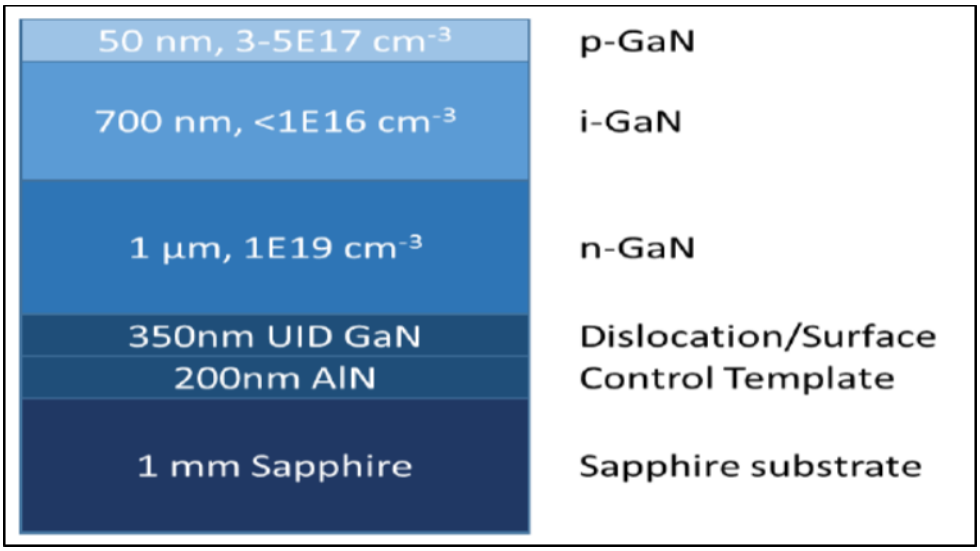

Figure 37: Fabricated device layers (not to scale)

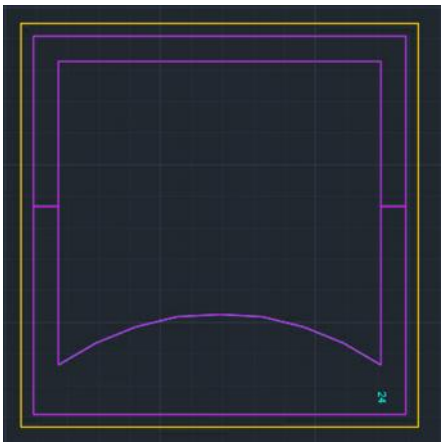

Figure 38: Device prototype design CAD image

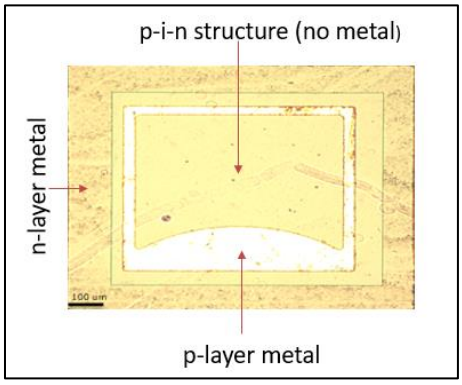

Figure 39: Optical image of fabricated prototype

The major fabrication steps included:

1. Photolithography and ICP etch to expose n-layer
2. Evaporate metal (Ti/Al/Ni/Au) on the n-layer for negative terminal
3. Rapid Thermal Anneal (750°C, 30s)
4. Evaporate metal (Ni/Au) on p-layer for positive terminal
5. Rapid Thermal Anneal (500°C, 60 s)
6. Evaporate metal (Ti/Au) for wire-bonding and packaging

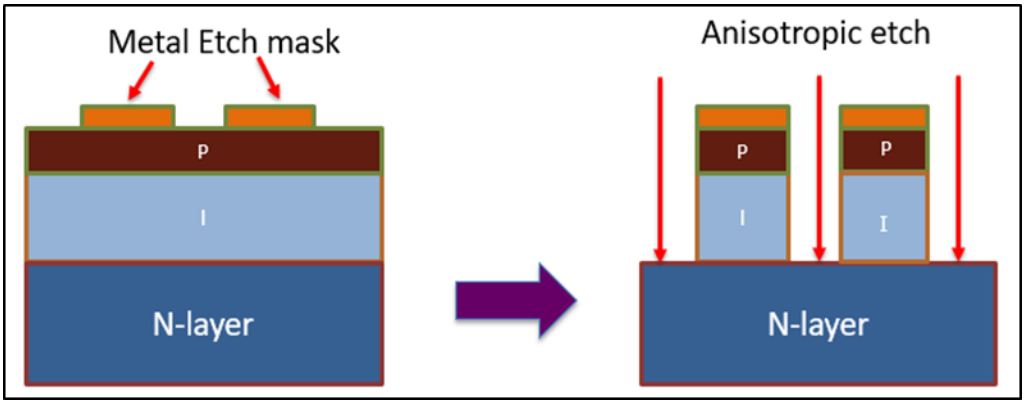

Figure 40: Fabrication etching step schematic

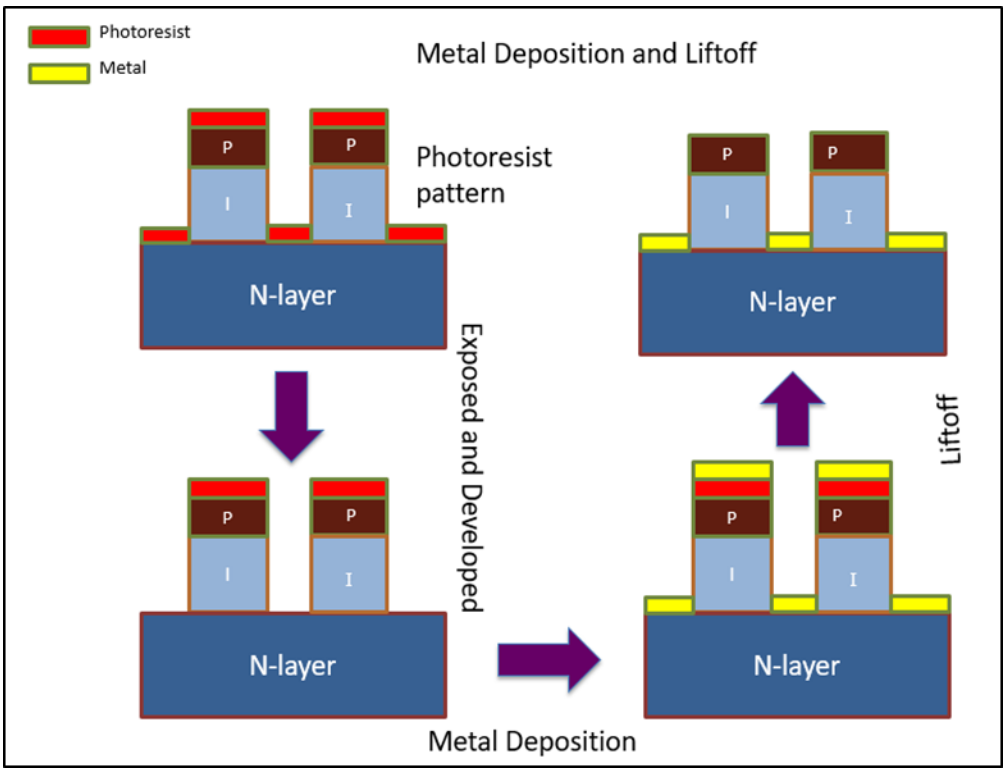

Figure 41: Fabrication metal deposition schematic

Device Characterization Utilizing Dark IV Measurements

We characterized our fabricated devices using current - voltage (IV) measurements without illumination (light or beta); using an electron beam at various accelerating voltages to simulate its behavior as a betavoltaic microbattery. IV measurements were performed in a Wentworth PML 8000 probe station at room temperature using an Agilent 4155 semiconductor parameter analyzer. The device was tested in a forward bias by sweeping the voltage from 0 V to 10 V and from 0 V to -10 V for reverse bias. Figure 42 shows the I-V characteristics of a device over a voltage range of – 10 V to + 10 V. This fabricated GaN p-i-n device shows rectification as expected from a diode and the turn-on voltage is roughly 3.2V. The turn on voltage is defined as the voltage at which the diode starts to conduct current. Under reverse bias the device has high leakage current density (700 mA at -10V) that is likely caused by tunneling through defects in the p-n junction.

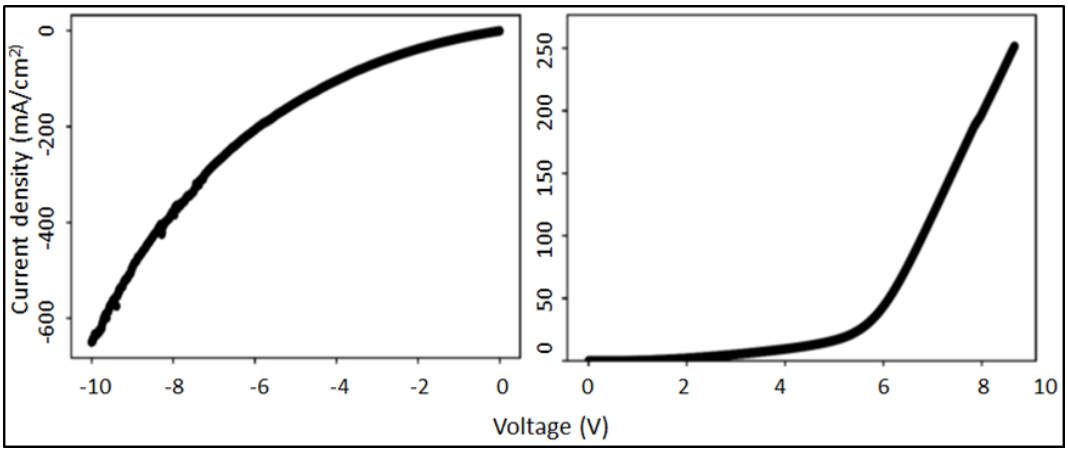

Figure 42: Dark IV characteristic experimental results in reverse and forward bias

Electron beam measurement is similar to dark IV measurement, utilizing an electron beam on the top side of the device to simulate beta exposure. The monochromatic electron beam's input current was fixed at 1 nA and the accelerating voltage was varied from 1 kV to 18 kV. We calculated the output power for tritium (5.6 keV) and Ni-63 (17 keV) by multiplying the resulting short circuit current (Isc) with open circuit voltage (Voc). Figure 43 shows the resulting output power as a function of incident beam energy for this device. Output power of 7.2 nW was generated at the average energy emission of tritium (5.6 keV) and output power of 9.9 nW at the average energy emission for Ni-63 (17 keV).

Conclusion

We experimentally demonstrated a betavoltaic power source with applications to MEMS blast sensors, which can potentially be used to recharge an existing battery in order to extend its useful life. The output power simulated from this device is very small (nano-Watts regime), but it is a constant power source which could potentially be used with a capacitor to store charge for later use on demand. We fabricated 20 devices, which performed as expected in dark IV testing in the forward bias direction. However, reverse bias testing showed signs of high leakage current, which is important because it reduces the output power and efficiency of GaN energy conversion devices. Due to resource constraints, we were only able to test a single device under the electron-beam to simulate its behavior for beta sources, tritium and Nickel-63, however this device produced output power of 7.2 nW and 9.9 nW for tritium and Ni-63 sources, respectively. In future work our design could be optimized for increased output power by utilizing GaN grown on a GaN p-i-n structure. Currently, our GaN is grown on a sapphire structure, which is mismatched to the GaN lattice, and is a source of decreased efficiency in our fabricated devices. We would like to thank Marc Litz and Randy Tompkins of the US Army Research Laboratory for their collaboration on this effort.

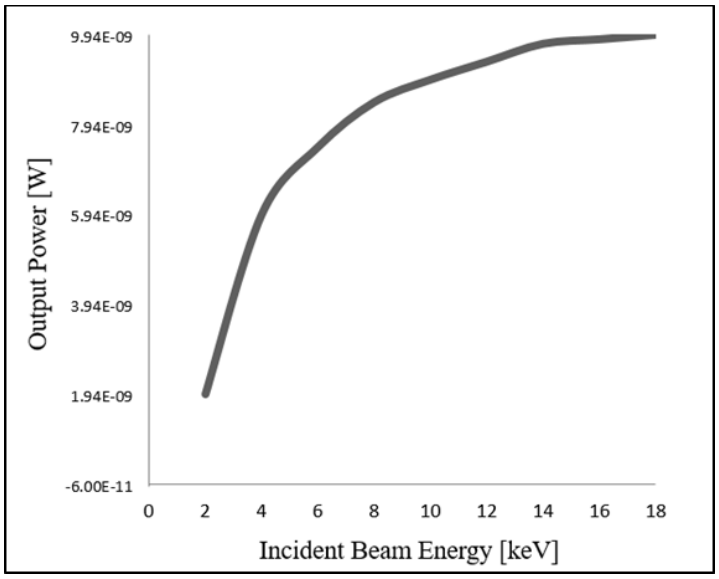

Figure 43: Electron beam experimental results: output power vs. incident beam energy

References

1. W. Ehrenber, et al., "The Electron Voltaic Effect" Proc. Rody. Soc. 64, 424 (1951)
2. Rappaport, P., The electron-voltaic effect in p-n junctions induced by betaparticle bombardment. Physical Review, 1954. 93(1): p. 246-247
3. Huffman, F. and J. Norman, Nuclear-fueled cardiac pacemakers. Chest, 1974. 65(6): p. 667.
4. Eiting, C., et al., Demonstration of a radiation resistant, high efficiency SiC betavoltaic. Applied Physics Letters, 2006. 88: p. 064101.
5. Chandrashekhar, M., et al., Demonstration of a 4H SiC betavoltaic cell. Applied Physics Letters, 2006. 88: p. 033506
6. Andreev V M, K E Bower, Y A Barbanel, Y G Shreter and G W Bohnert, Polymers, Phosphors, and Voltaics for Radioisotope Batteries, Boca Raton, FL: CRC Press, p 48 (2002).

DISTRIBUTION

Internal:

TECHNICAL LIBRARY
INFORMATION MANAGEMENT DIVISION
(D1), BLDG. 2172
6013 HOWARD ROAD, RM 223
INDIAN HEAD MD 20640-4622
IHDIVTECHNICALLIBRARY@NAVY.MIL

Electronic Copy:

ADMINISTRATOR
DEFENSE TECH INFORMATION CTR
ATTN CHRISTINE BARRETT
8725 JOHN J KINGMAN RD STE 0944
FT BELVOIR VA 22060-6218
CHRISTINE.E.BARRETT.CIV@DTIC.MIL
703.767.9011

This page intentionally left blank.